On phase separation and crystallization of Ge-rich GeSbTe alloys from atomistic simulations with a machine learning interatomic potential // Supplementary Information

Omar Abou El Kheir, Dario Baratella and Marco Bernasconi

Department of Materials Science, University of Milano-Bicocca
Via R. Cozzi 55, I-20125 Milano, Italy

Contents

1 Database

In Table S1 we report on the number of configurations for each compound/alloy in the database, the cell size, the Root Mean Square Error (RMSE) on energy and forces for both the training and test datasets. Similarly, in Table S2 we report on the same information for the transferability test set on compositions not included in the training database. Moreover, in Fig. S1a-b we report on the cumulative fraction of the absolute errors of the NN potential in training and test data sets of GST523 on the energies per atom and forces, while in Fig. S1c we report on the distribution of the absolute error as a function of DFT energy. The training database conists of about 470,000 configurations of small cells in the amorphous and liquid phases and in the crystalline phases only for the elemental and stoichiometric compounds. The database for GST523 also include configurations of Ge-GeSbTe interfaces generated by metadynamics simulations designed to accelerate the segregation of Ge in GGST alloys (see article).

Composition	Number of configurations	cell size (atoms)	RMSE on energy Training/Test (meV/atom)	RMSE on Forces Training/Test (eV/Å)
Ge	39132	64-144	6.6 (6.6)	0.143 (0.141)
Sb	19011	54-72	6.0 (5.9)	0.124 (0.123)
Te	17354	64-162	13.3 (12.2)	0.200 (0.189)
GeSb	21005	64-72	5.6 (5.5)	0.132 (0.131)
$Ge_{15}Sb_{85}$	10042	64	6.1 (5.9)	0.128 (0.128)
GeTe	42900	96-108	7.8 (8.0)	0.141 (0.142)
Ge_2Te	51300	100	8.2 (8.2)	0.152 (0.152)
Sb_2Te	8819	72-81	5.9 (5.9)	0.161 (0.159)
Sb_2Te_3	9649	60-135	11.4 (11.5)	0.186 (0.188)
$GeSb_2Te_4$	7048	56	5.7 (5.9)	0.141 (0.141)
$Ge_2Sb_2Te_5$	183654	98-216	8.8 (9.2)	0.155 (0.156)
$Ge_5Sb_2Te_3$	47315	150	4.0 (4.0)	0.142 (0.142)
SL	11700	68-76	2.2 (2.2)	0.084 (0.084)

Table S1: Number of configurations included in the database for each composition, cell size and the average RMSE on energy and forces for training (test) subset. SL refer to superlattices of crystalline: GeTe-GST225, Sb_2Te_3-GST225 and GST326-GST124.

Composition	Number of configurations	cell size (atoms)	RMSE on energy Test (meV/atom)	RMSE on Forces Test (eV/Å)
$GeSb_8Te$	5010	100	7.9	0.139
$Ge_3Sb_4Te_3$	5010	100	6.6	0.145
$Ge_4Sb_2Te_4$	5010	100	11.0	0.149
$Ge_5Sb_3Te_2$	5010	100	6.0	0.143
$Ge_5Sb_4Te_1$	5010	100	12.0	0.144
$Ge_{7.4}Sb_{1.3}Te_{1.3}$	5010	100	8.2	0.141
Ge_2Te interfaces	800	300	8.83	0.143
Ge_3Te	2000	300	13.5	0.146
Ge_9Te	2000	300	10	0.137

Table S2: Number of configurations in the transferability data set for each composition, cell size and the average RMSE on energy and forces for test datasets. The configurations refer to the liquid and amorphous phases for all compositions. Ge_2Te interfaces refer to configurations of the interface between Ge_2Te and Ge taken from Ref. [1].

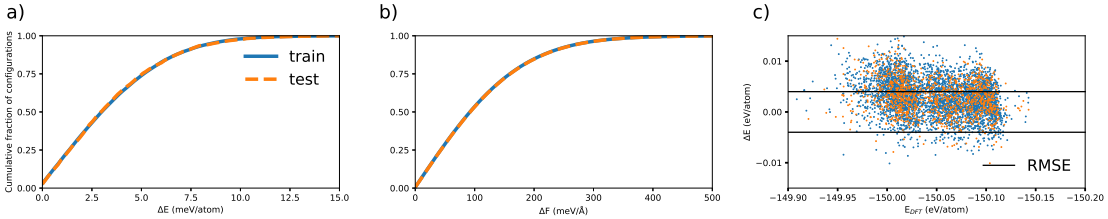

Figure S1: Cumulative fraction of the absolute errors of the NN potential in training and test data sets of GST523 (a) the energies per atom (ΔE=|E_{DFT}-E_{NN}|) and (b) forces (ΔF=|F_{DFT}-F_{NN}|). c) The distribution of the absolute error as a function of DFT energy.

2 Validation of the potential

Hereafter, we report the validation of the NN potential on structural, dynamical and thermodynamical properties of GeSbTe alloys. To study the liquid phase, we first prepared a model equilibrated at 2000 K for 20 ps for each alloy. Then, the models were quenched in 20 ps down to a target temperature (T_{target}) in 30 ps and finally the models were equilibrated at the T_{target} for 50 ps before evaluating the average properties. T_{target}, in the range 1200-990 K, was chosen for each alloy to be higher than the melting temperature.

2.1 $Ge_2Sb_2Te_5$

The structural properties of the liquid $Ge_2Sb_2Te_5$ (GST225) at the experimental density of the amorphous phase (0.0309 atoms/Å^3)[2] obtained from Neural Network molecular dynamics (NN-MD) simulation with a 999-atom model at 990 K are compared with those obtained from DFT-MD simulation with a 216-atom model from Ref. [3] at the same density (see Fig. S2). The structural properties were averaged over trajectories 50 ps long. The pair correlation functions, the bond angles distribution function and the distribution of coordination numbers are compared with DFT results in Fig. S2. The position of the first maximum and minimum of each partial correlation function are given in Table S3. We also validated the NN potential over the dynamical properties of the liquid/supercooled phase down to 650 K, by comparing the self diffusion coefficient (D) from NN-MD simulation with DFT results from Ref. [4] (See Fig. S2d). Then we validated the NN potential on the structural properties of the amorphous phase at the same density. The 999-atom liquid model was quenched from the melt at 990 K to 300 K in 100 ps, and equilibrated at 300 K for 40 ps. Structural properties were averaged over a subsequent run 50 ps long. In Fig. S3, structural properties from NN-MD are compared with those obtained from

amorphous model generated with DFT-MD simulation in Ref. [3] with a similar protocol. The pair correlation functions, the bond angle distribution function, the distribution of coordination numbers and the distribution of the local order parameter q for tetrahedricity for four-coordinated Ge atom are compared to DFT results in Fig. S3. The position of the first maximum and minimum of each partial correlation function are given in Table S4, while the average coordination number for different pairs of atoms are given in Table S5. In the amorphous phase of GST225, four-coordinated Ge atoms are in defective octahedral geometry and in tetrahedral configurations. The fraction of Ge atoms tetrahedral configuration can be quantified by integrating the q order parameter between 0.8 and 1 as was discussed in previous works [3]. In the NN model, 22% of Ge atoms are in tetrahedral configuration, to be compared with 23% from DFT models reported in Ref. [3]. Finally, the NN potential was validated on the structural properties of the hexagonal and cubic crystalline phases of GST225 by fitting the equation of state (EOS) at zero temperature of both phases by fitting the energy vs volume data with the Birch–Murnaghan formula (see Figs. S4 and S5). The resulting parameters at equilibrium are compared with DFT data in Tables S6 and S7. Overall, the structural properties obtained from NN-MD simulations are in excellent agreement with those obtained from DFT-MD, which suggests that the NN potential reliably describes the properties of the different phases of GST225.

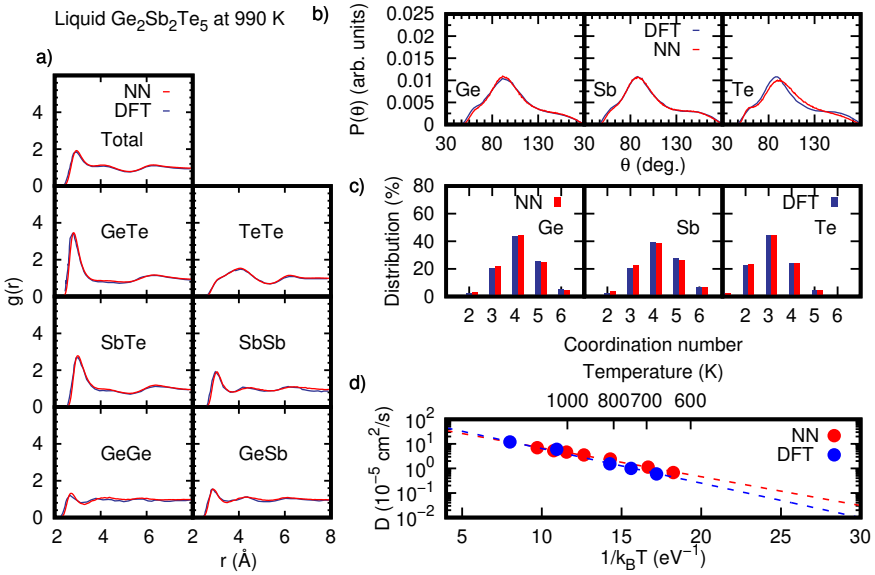

Figure S2: Structural and dynamical properties of liquid GST225 from DFT (blue curves) and NN (red curves) simulations with a 216-atom or 999-atom models, respectively. a) Total and partial radial distribution functions at 990 K. The position of the first maximum and minimum of each partial correlation function are given in Table S3. b) Angle distribution function resolved per central atomic species at 990 K. The data were normalized to the number of triplets in each model. c) Distribution of coordination numbers resolved per chemical species at 990 K computed by integrating the partial pair correlation functions up to a bonding cutoff which corresponds to 3.2 Å for all pairs except for Sb–Te for which we use 3.4 Å. We use the same bonding cutoff of the amorphous phase. d) The Arrhenius plot of the diffusion coefficient D as a function of temperature compared with previous DFT results with the PBE functionals from Ref. [3]

Table S3: First maximum and minimum of the pair correlation functions in liquid GST225 at 990 K from NN-MD and DFT-MD (in parenthesis) simulations. Details on the simulation cells are given in the caption of Fig. S2.

Bond type	First maximum (Å)	First minimum (Å)
GeGe	2.71 (2.70)	3.29 (3.24)
GeSb	2.86 (2.88)	3.51 (3.6)
GeTe	2.81 (2.80)	-
SbSb	3.04 (3.00)	3.72 (3.78)
SbTe	3.00 (3.04)	-
TeTe	-	-

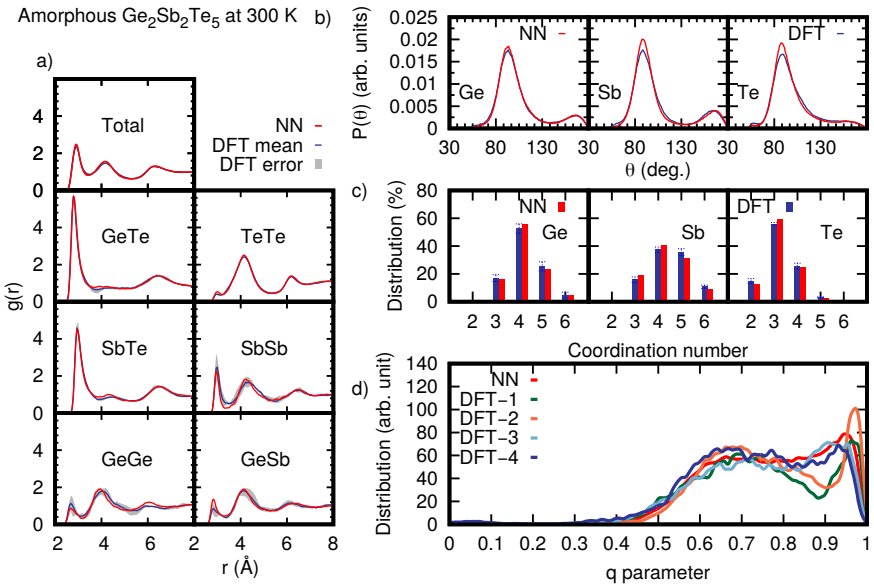

Figure S3: Structural properties of amorphous GST225 at 300 K from NN (red curves) and DFT (blue curves) simulations. DFT data are averaged over four independent 216-atom models while NN data are obtained from a 999-atom model. a) Total and partial radial distribution functions. The position of the first maximum and minimum of the different functions is reported in Supplementary Table S4. b) Angular distribution function resolved per central atomic species. The data are normalized to the number of triplets in each model. c) Distribution of coordination numbers resolved per chemical species, obtained by integrating the pair correlation functions up to a bonding cutoff corresponding to 3.2 Å for all pairs except for Sb-Te for which a longer cutoff value of 3.4 Å was used. The spread over the four DFT models are indicated by error bars. d) Distribution of the local order parameter q for tetrahedricity for four-coordinated Ge atoms for the NN model and for each of our four DFT models.

Table S4: Position (Å) of the first maximum and minimum of the pair correlation functions in the amorphous phase of GST225 at 300 K from DFT and NN simulations. DFT data are given in parenthesis.

Bond type	First maximum (Å)	First minimum (Å)
GeGe	2.64 (2.66)	3.14(3.15)
GeSb	2.82 (2.83)	3.3 (3.3)
GeTe	2.78 (2.78)	-
SbSb	2.92 (2.99)	-
SbTe	2.92 (2.97)	-
TeTe	3.00 (2.99)	-

Table S5: Average coordination numbers for different pairs of atoms in amorphous GST225 at 300 K generated from DFT (in parenthesis) and NN simulations. Error bars for DFT data are obtained from the analysis of four models. Details on the simulation cells and bonding cutoff are given in the caption of Fig. S3.

-	Ge	Sb	Te
Total	4.16 (4.17±0.1)	4.29 (4.40±0.05)	3.17 (3.16±0.05)
With Ge	0.28 (0.34±0.05)	0.34 (0.26±0.05)	1.42 (1.42±0.02)
With Sb	0.34 (0.26±0.05)	0.41 (0.51±0.1)	1.42 (1.45±0.05)
With Te	3.54 (3.57±0.05)	3.54 (3.63±0.1)	0.34 (0.28±0.02)

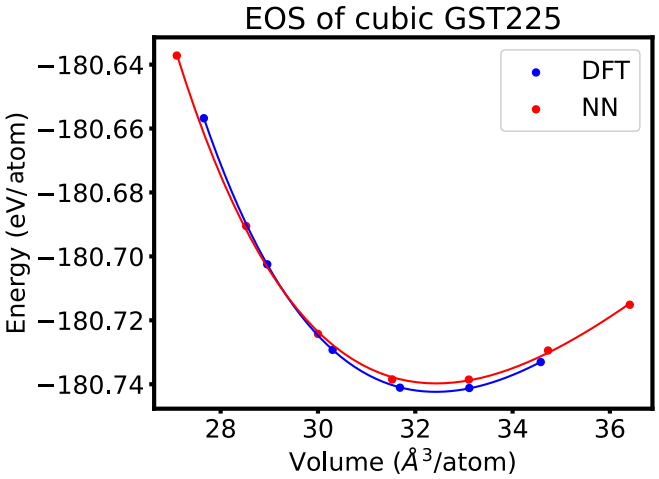

Figure S4: Equation of state (EOS) of the cubic phase of GST225 from DFT and NN calculations.

Table S6: Fitting parameters of the Birch-Murnaghan equation of state of cubic GST225 from NN and DFT-PBE calculations at zero temperature. The energy (E_0), volume (V_0), bulk modulus (B) and derivative of B (B') at equilibrium are reported.

	E_0 (eV atom^{-1})	V_0 (Å^3 atom^{-1})	B (GPa)	B'
DFT	-180.7424	32.42	25.1	7.53
NN	-180.7400	32.34	22.88	7.49

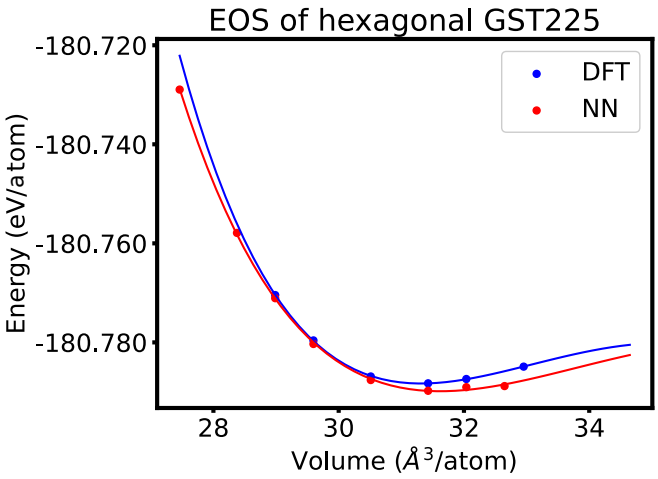

Figure S5: Equation of state (EOS) of the hexagonal phase of GST225 (Kooi stacking [5], see article) from DFT and NN calculations.

Table S7: Fitting parameters of the Birch-Murnaghan equation of state of hexagonal GST225 from NN and DFT-PBE calculations at zero temperature. The energy (E_0), volume (V_0), bulk modulus (B) and derivative of B (B') at equilibrium are reported.

	E_0 (eV atom^{-1})	V_0 (Å^3 atom^{-1})	B (GPa)	B'
DFT	-180.7883	31.31	19.8	21.75
NN	-180.7890	31.61	16.5	18.5

2.2 $Ge_5Sb_2Te_3$

As no experimental data are available for the density of amorphous $Ge_5Sb_2Te_3$ (GST523), we have modeled GST523 at the theoretical density of 0.0338 atom/Å obtained from DFT+D3 MD simulations in Ref. [6]. However, in this section, we first report on structural properties from NN-MD and DFT-MD with no vdW corrections for the sake of validating our NN potential fitted on a DFT-PBE database. The structural properties of the liquid GST523 at the theoretical density of amorphous phase obtained from NN-MD simulation with a 1760-atom model at 1000 K are compared to those obtained from DFT-MD simulation with a 220-atom model at the same density (see Fig. S6). The structural properties were averaged over a trajectory 50 ps long. The pair correlation functions, the bond angles distribution function and the distribution of coordination numbers are compared with DFT results in Fig. S6. Then, we validated the NN potential on the structural properties of the amorphous phase at the same density. The 1760-atom liquid model was quenched from the melt from 1000 K to 300 K in 100 ps, and then equilibrated at 300 K for 40 ps.

The structural properties were averaged over a subsequent run 50 ps long. In Fig. S7, the structural properties from NN-MD are compared with those obtained from the amorphous model generated by DFT-MD with a similar protocol. The pair correlation functions, the bond angles distribution function, the distribution of coordination numbers and the distribution of the local order parameter q for tetrahedricity for four-coordinated Ge atom are compared with DFT results in Fig. S7. The average coordination number for different pairs of atoms are given in Table S8. We also quantified the fraction of four-coordinated Ge atoms in tetrahedral geometry by integrating the distribution of the q parameter between 0.8 and 1 as discussed previously, resulting in 38% in the NN model compared to 44% in the DFT model. Once again, the structural properties obtained from NN-MD simulations are in excellent agreement with those obtained from DFT-MD which suggests that the NN potential reliably describes the properties of the different phases of GST523.

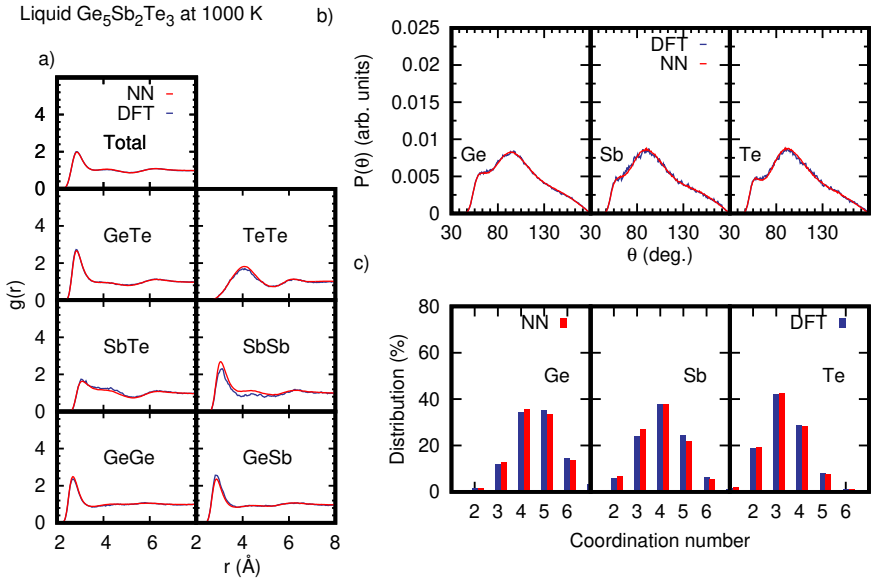

Figure S6: Structural properties of liquid GST523 at 1000 K from NN (red curves) and DFT (blue curves) simulations. NN (DFT) data refer to a 1760-atom (220-atom) model. a) Total and partial pair correlation functions. b) Angular distribution function resolved per central atomic species. The data are normalized to the number of triplets in each model. c) Distribution of coordination numbers resolved per chemical species, obtained by integrating the pair correlation functions up to a bonding cutoff corresponding to 3.2 Å for all pairs except for Sb-Te for which a longer cutoff value of 3.4 Å was used which correspond to the same cutoff used for the amorphous phase.

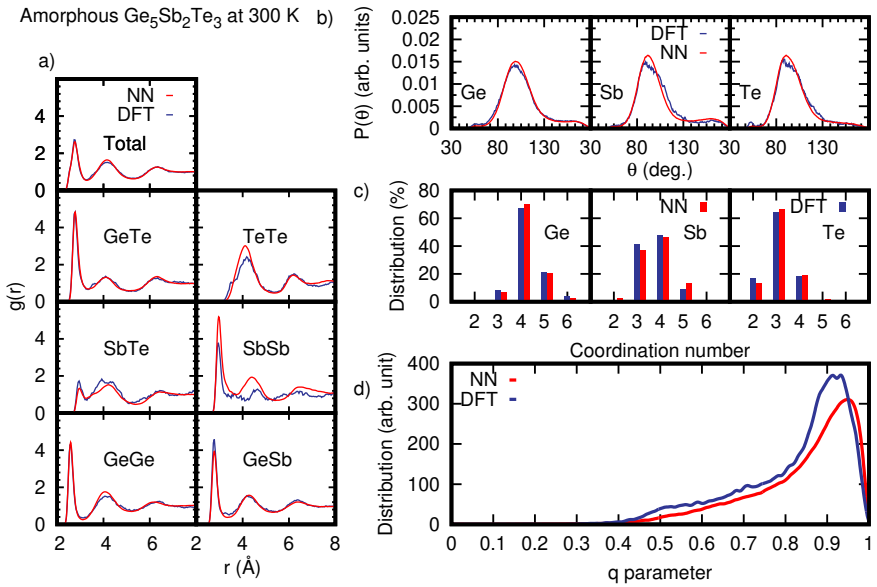

Figure S7: Structural properties of amorphous GST523 at 300 K from NN (red curves) and DFT (blue curves) simulations. NN (DFT) data refer to a 1760-atom (220-atom) model. a) Total and partial radial distribution functions. b) Angular distribution function resolved per central atomic species. The data are normalized to the number of triplets in each model. c) Distribution of coordination numbers resolved per chemical species, obtained by integrating the pair correlation functions up to a bonding cutoff corresponding to 3.2 Å for all pairs except for Sb-Te for which a longer cutoff value of 3.4 Å was used. d) Distribution of the local order parameter q for tetrahedricity for four-coordinated Ge atoms for the NN model and for each of our four DFT models. The large misfit in the Sb-Sb pair correlation function is due to the poor statistics in the small 220-atom cell for this composition with a low fraction of Sb.

Table S8: Average coordination numbers for different pairs of atoms in amorphous GST523 at 300 K generated from DFT (in parenthesis) and NN simulations. Details on the simulation cells and bonding cutoff are given in the caption of Fig. S7

-	Ge	Sb	Te
Total	4.18 (4.20)	3.73 (3.68)	3.08 (3.03)
With Ge	1.86 (1.86)	1.92 (2.11)	2.59 (2.49)
With Sb	0.77 (0.84)	1.08 (0.77)	0.48 (0.53)
With Te	1.55 (1.49)	0.72 (0.79)	0.001 (0.005)

We also computed the structural properties by including the vdW interaction D3

for the amorphous phase as discussed above. The NN+D3 data are compared to the DFT+D3 results from Ref. [6] in Fig. S8

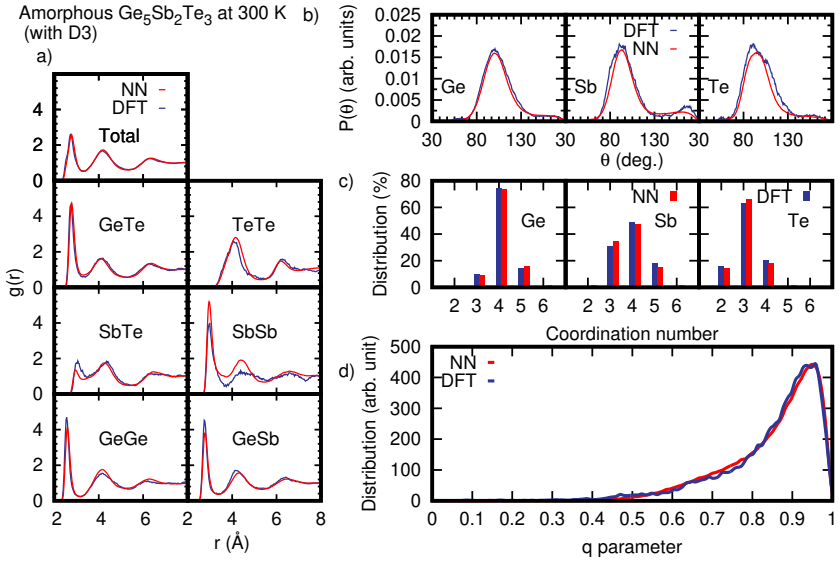

Figure S8: Structural properties of amorphous GST523 at 300 K from NN+D3 (red curves) and DFT (blue curves) simulations. NN (DFT) data refer to a 1760-atom (220-atom) model. a) Total and partial radial distribution functions. b) Angular distribution function resolved per central atomic species. The data are normalized to the number of triplets in each model. c) Distribution of coordination numbers resolved per chemical species, obtained by integrating the pair correlation functions up to a bonding cutoff corresponding to 3.2 Å for all pairs except for Sb-Te for which a longer cutoff value of 3.4 Å was used. d) Distribution of the local order parameter q for tetrahedricity for four-coordinated Ge atoms.

2.3 *GeTe*

The structural properties of the liquid GeTe at the experimental density of amorphous phase (0.0333 atoms/Å^3)[7] obtained from NN-MD simulation with a 4096-atom model at 1150 K are compared with those obtained from DFT-MD simulation with a 300-atom model from Ref. [1] at the same density (see Fig. S9). The structural properties were averaged over a trajectory 50 ps long. The pair correlation functions, the bond angles distribution function and the distribution of coordination numbers are compared with DFT results in Fig. S9. Then, we validated the NN potential on the structural properties of the amorphous phase at the same density. The 4096-atom liquid model was quenched from the melt at 1150 K to 300 K in 100 ps, and equilibrated for 40 ps at 300 K. Structural properties are averaged over a

subsequent run 50 ps long. In Fig. S10, the structural properties from NN-MD are compared with those obtained from an amorphous model generated by DFT-MD simulation in Ref. [1] with a similar protocol. The pair correlation functions, the bond angles distribution function, the distribution of coordination numbers and the distribution of the local order parameter q for tetrahedricity for four-coordinated Ge atom are compared with DFT results in Fig. S10. The average coordination number for different pairs of atoms are given in Table S9. We also quantified the fraction of four-coordinated Ge atoms in tetrahedral geometry by integrating the distribution the q parameter between 0.8 and 1 as discussed in previously, resulting in 21% in NN model compared to 24% in DFT results from Ref. [1]. Finally, the NN potential was validated on the structural properties of the trigonal crystal phase of GeTe by fitting the EOS (see Figs. S11). The resulting parameters at equilibrium are compared with DFT data in Tables S10. Similarly to GST225 and GST523, the structural properties of GeTe obtained from NN-MD simulations are in a good agreement with those obtained from DFT-MD, so we conclude that the NN potential can reliably describe the properties of the different phases of GeTe.

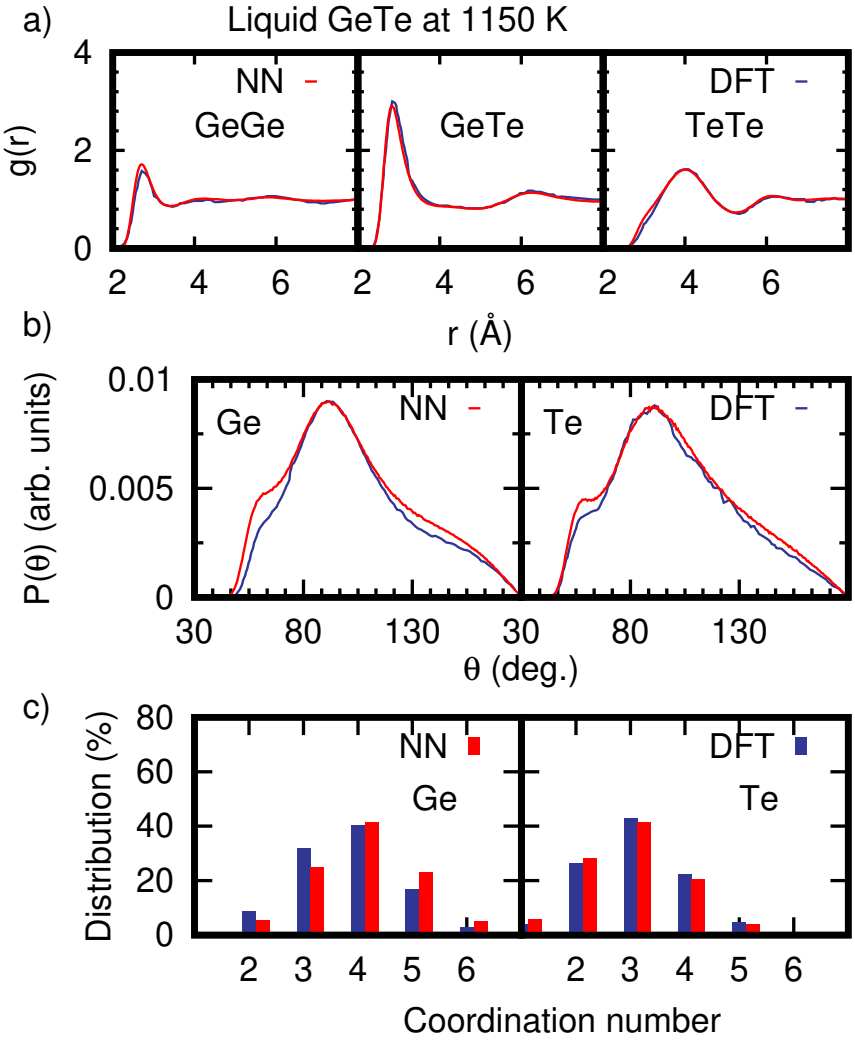

Figure S9: Structural properties of liquid GeTe at 1150 K from NN (red curves) and DFT (blue curves) simulations. NN (DFT) data refer to a 4096-atom (300-atom) model. a) Total and partial radial distribution functions. b) Angular distribution function resolved per central atomic species. The data are normalized to the number of triplets in each model. c) Distribution of coordination numbers resolved per chemical species, obtained by integrating the pair correlation functions up to a bonding cutoff of 3.0 Å for Ge-Ge and Te-Te and of 3.22 Å for Ge-Te. of the We used the same cutoff values of the amorphous phase.

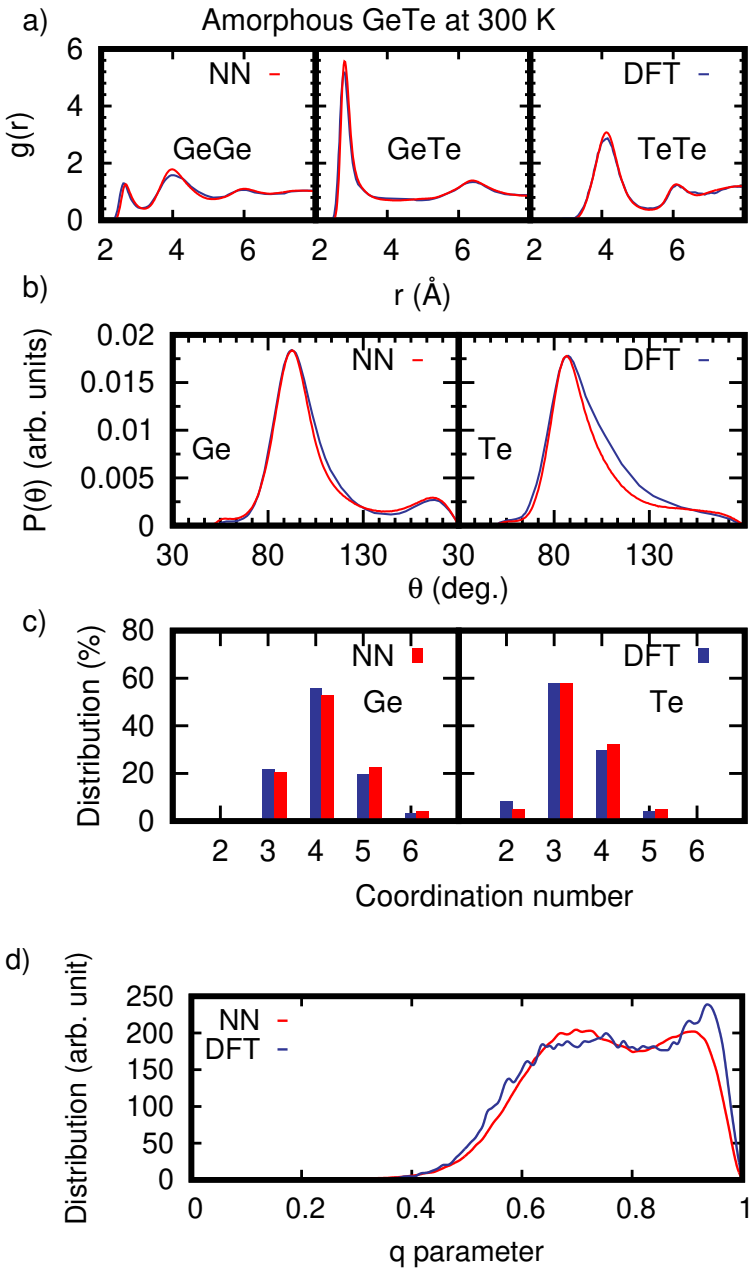

Figure S10: Structural properties of amorphous GeTe at 300 K from NN (red curves) and DFT (blue curves) simulations. NN (DFT) data refer to a 4096-atom (300-atom) model. a) Total and partial radial distribution functions. b) Angular distribution function resolved per central atomic species. The data are normalized to the number of triplets in each model. c) Distribution of coordination numbers resolved per chemical species, obtained by integrating the pair correlation functions up to a bonding cutoff of 3.0 Å for Ge-Ge and Te-Te and of 3.22 Å for Ge-Te. d) Distribution of the local order parameter q for tetrahedricity for four-coordinated Ge atoms.

Table S9: Average coordination numbers for different pairs of atoms in amorphous $GeTe$ at 300 K generated from DFT (in parenthesis) and NN simulations. Details on the simulation cells and bonding cutoff are given in the caption of Fig. S10.

-	Ge	Te
Total	4.09 (4.04)	3.38 (3.21)
With Ge	0.71 (0.87)	3.37 (3.18)
With Te	3.37 (3.18)	0.01 (0.04)

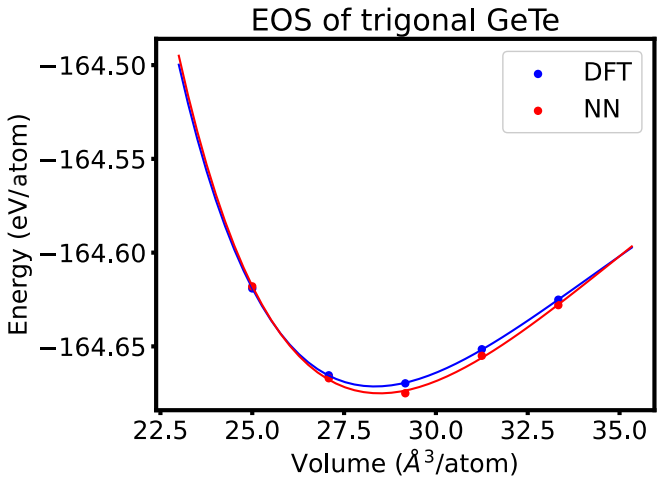

Figure S11: Equation of state (EOS) of the trigonal phase of GeTe from DFT and NN calculations.

Table S10: Fitting parameters of the Birch-Murnaghan equation of state of hexagonal GeTe from NN and DFT-PBE calculations at zero temperature. The energy (E_0), volume (V_0), bulk modulus (B) and derivative of B (B') at equilibrium are reported.

	E_0 (eV atom^{-1})	V_0 (Å^3 atom^{-1})	B (GPa)	B'
DFT	-164.671	28.34	28.88	8.55
NN	-164.675	28.47	29.61	7.93

2.4 Ge_2Te

Similarly to GST523, in the lack of experimental data for the density of Ge_2Te, we have modeled this alloy at the theoretical density of 0.0355 atom/Å^3 obtained from

DFT+D3 MD simulations in Ref. [1]. Yet, in this section we report on structural properties from NN-MD and DFT-MD with no vdW corrections for the sake of validating the fitting the NN potential fitted on a DFT-PBE database. The structural properties of the liquid Ge_2Te at the theoretical density of amorphous phase (0.0355 atoms/Å^3) obtained from NN-MD simulation with a 2400-atom model at 1200 K are compared with those obtained from DFT-MD simulation with a 300-atom model from Ref. [1] at the same density (see Fig. S12). The structural properties were averaged over a trajectory 50 ps long. The pair correlation functions, the bond angles distribution function and the distribution of coordination numbers are compared with DFT results in Fig. S12. Then, we validated the NN potential on the structural properties of the amorphous phase at the same density. The 4096-atom liquid model was quenched from the melt at 1200 K to 300 K in 100 ps, and equilibrated at 300 K for 40 ps. Structural properties averaged over a subsequent run 50 ps long. In Fig. S13, the structural properties from NN-MD are compared with those obtained from an amorphous model generated by DFT-MD simulation in Ref. [1] with similar protocol. The pair correlation functions, the bond angles distribution function, the distribution of coordination numbers and the distribution of the local order parameter q for tetrahedricity for four-coordinated Ge atom are compared with DFT results in Fig. S13. The average coordination number for different pairs of atoms are given in Table S11. We also quantified the fraction of four-coordinated Ge atoms in tetrahedral geometry by integrating the distribution of the q parameter between 0.8 and 1 as discussed previously, resulting in 43% in NN model compared to 52% in DFT results from Ref. [1]. Again, the structural properties of Ge_2Te obtained from NN-MD simulations are in a good agreement with those obtained from DFT-MD across the different phases of this alloy.

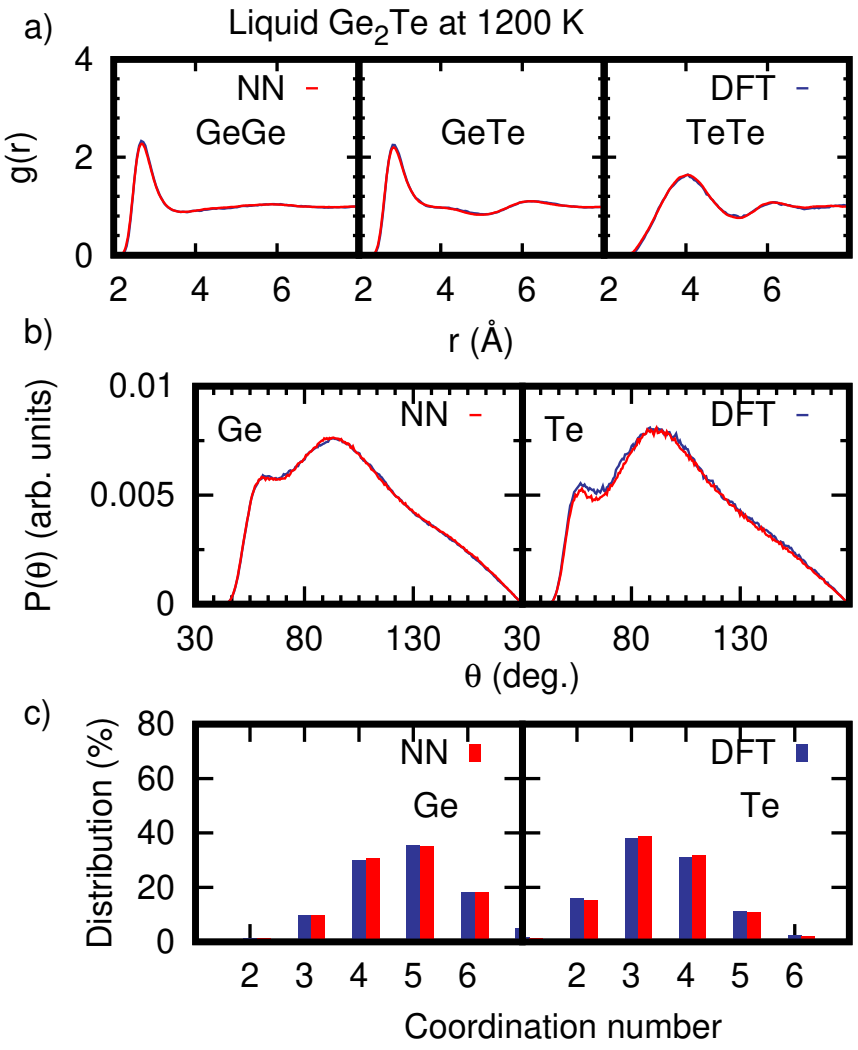

Figure S12: Structural properties of liquid Ge_2Te at 1200 K from NN (red curves) and DFT (blue curves) simulations. NN (DFT) data refer to a 2400-atom (300-atom) model. a) Total and partial radial distribution functions. b) Angular distribution function resolved per central atomic species. The data are normalized to the number of triplets in each model. c) Distribution of coordination numbers resolved per chemical species, obtained by integrating the pair correlation functions up to a bonding cutoff of 3.0 Å for Ge-Ge and Te-Te and of 3.22 Å for Ge-Te. We used the same cutoff values of the amorphous phase.

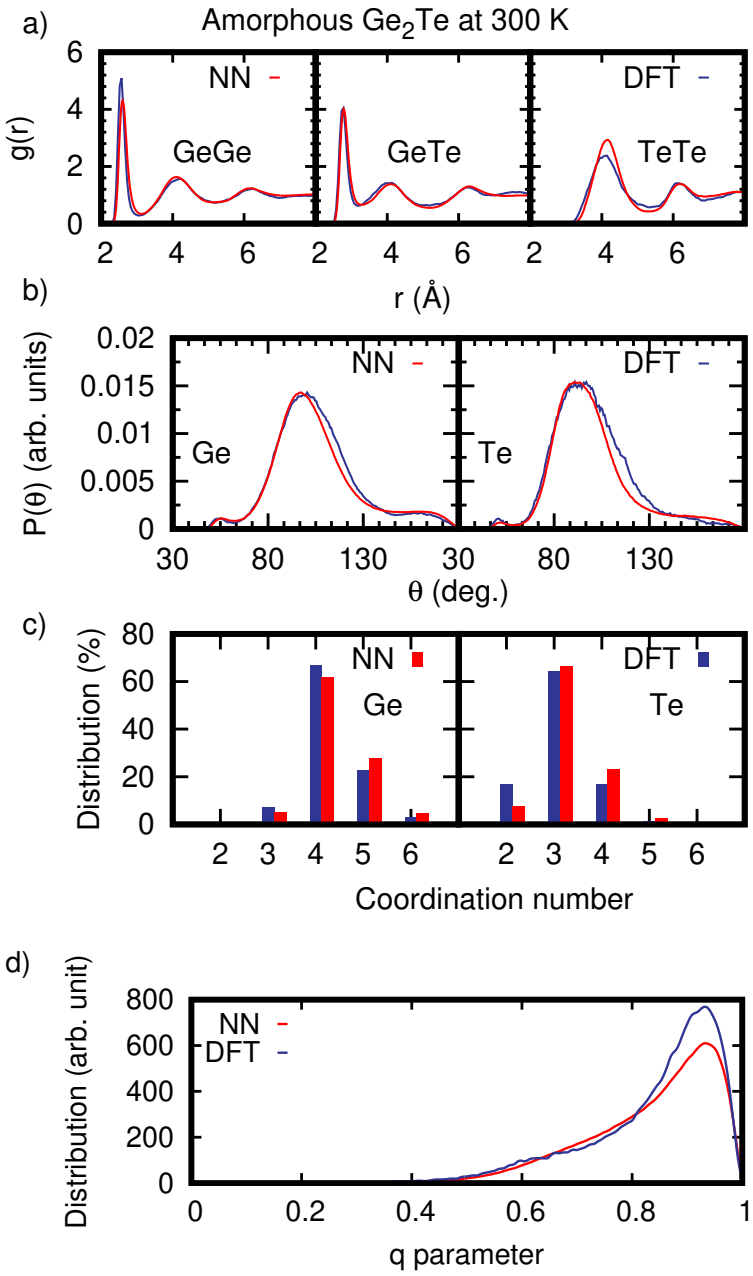

Figure S13: Structural properties of amorphous Ge_2Te at 300 K from NN (red curves) and DFT (blue curves) simulations. NN (DFT) data refer to a 2400-atom (300-atom) model. a) Total and partial radial distribution functions. b) Angular distribution function resolved per central atomic species. The data are normalized to the number of triplets in each model. c) Distribution of coordination numbers resolved per chemical species, obtained by integrating the pair correlation functions up to a bonding cutoff of 3.0 Å for Ge-Ge and Te-Te and of 3.22 Å for Ge-Te. d) Distribution of the local order parameter q for tetrahedricity for four-coordinated Ge atoms.

Table S11: Average coordination numbers for different pairs of atoms in amorphous Ge_2Te at 300 K generated from DFT (in parenthesis) and NN simulations. Details on the simulation cells and bonding cutoff are given in the caption of Fig. S13.

-	Ge	Te
Total	4.33 (4.04)	3.20 (2.96)
With Ge	2.75 (2.58)	3.19 (2.96)
With Te	1.57 (1.46)	0.01 (0.00)

2.5 *GeSb*

In the lack of experimental data for the density of GeSb, we have modeled this alloy at the theoretical density of 0.0352 atom/Å^3. This density was obtained from a NPT simulation with the NN+D3 at 1000 K. In this simulation, we first started with a density of 0.0368 atom/Å^3, 8% lower than the density of the crystal (0.04 atom/Å^3) as was suggested for GST225. After an equilibration MD simulation 30 ps long, we obtained the theoretical density as the average over 30 ps long trajectory which results in average density 0.0352 atom/Å^3 which is slightly lower than our initial estimate. We then verified that the residual stress at this density in the liquid at 1000 K is small in a DFT simulation 20 ps long, which is on average 0.89 GPa.

The structural properties of the liquid GeSb at the theoretical density of the liquid phase (0.0352 atoms/Å^3) obtained from NN-MD simulation with a 512-atom model at 1000 K are compared with those obtained from DFT-MD simulation with a 148-atom model at the same density (see Fig. S14). The structural properties were averaged over a trajectory 50 ps long. The pair correlation functions, the bond angles distribution function and the distribution of coordination numbers are compared with DFT results in Fig. S14. Then, we validated the NN potential on the structural properties of the amorphous phase at the same density. The 512-atom liquid model was quenched from the melt at 1000 K to 300 K in 100 ps, and equilibrated at 300 K for 40 ps. Structural properties are averaged over a subsequent run 50 ps long. In Fig. S15, the structural properties from NN-MD are compared with those obtained from amorphous model generated with DFT-MD with similar protocol. The pair correlation functions, the bond angles distribution function, the distribution of coordination numbers and the distribution of the local order parameter q for tetrahedricity for four-coordinated Ge atom are compared with DFT results in Fig. S15. The average coordination number for different pairs of atoms are given in Table S12. We also quantified the fraction of four-coordinated Ge atoms in tetrahedral geometry by integrating the distribution of the q parameter between 0.8 and 1 as discussed previously, resulting in 75% in the NN model to be compared to the value

of 63% in the DFT model.

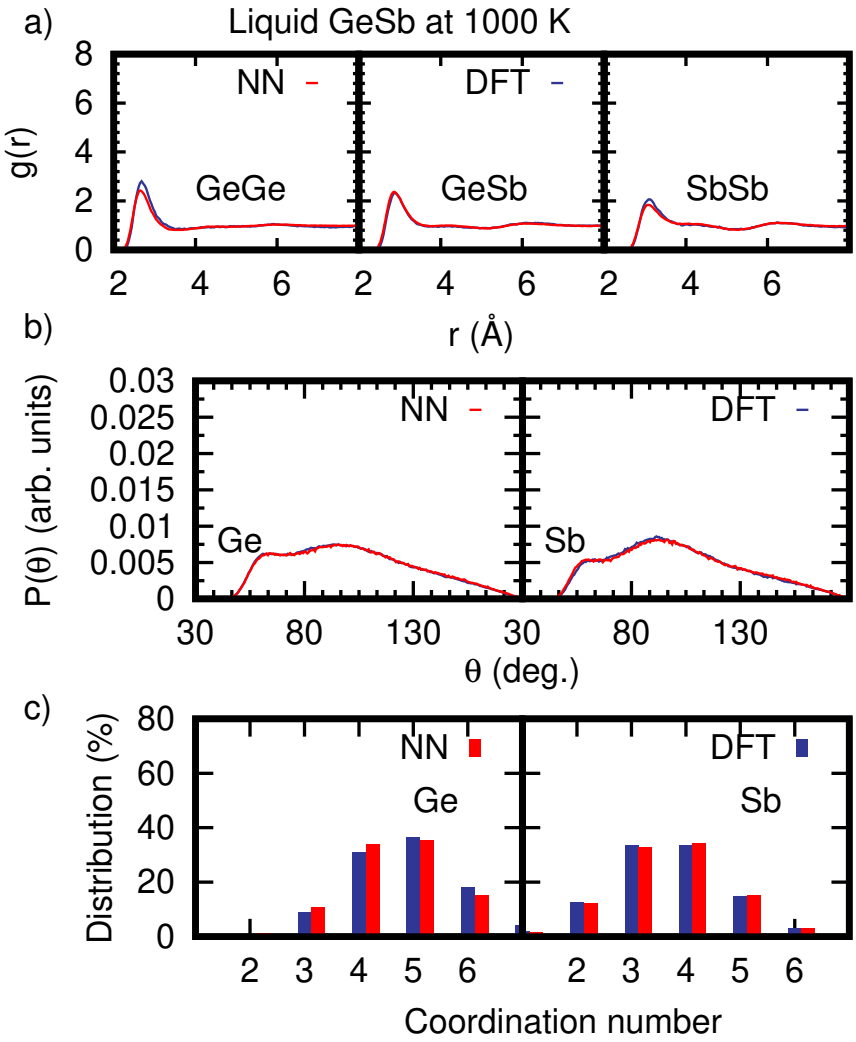

Figure S14: Structural properties of liquid GeSb at 1000 K from NN (red curves) and DFT (blue curves) simulations. NN (DFT) data refer to a 512-atom (148-atom) model. a) Total and partial radial distribution functions. b) Angular distribution function resolved per central atomic species. The data are normalized to the number of triplets in each model. c) Distribution of coordination numbers resolved per chemical species, obtained by integrating the pair correlation functions up to a bonding cutoff of 3.2 Å for all pairs. We used the same bonding cutoff of the amorphous phase.

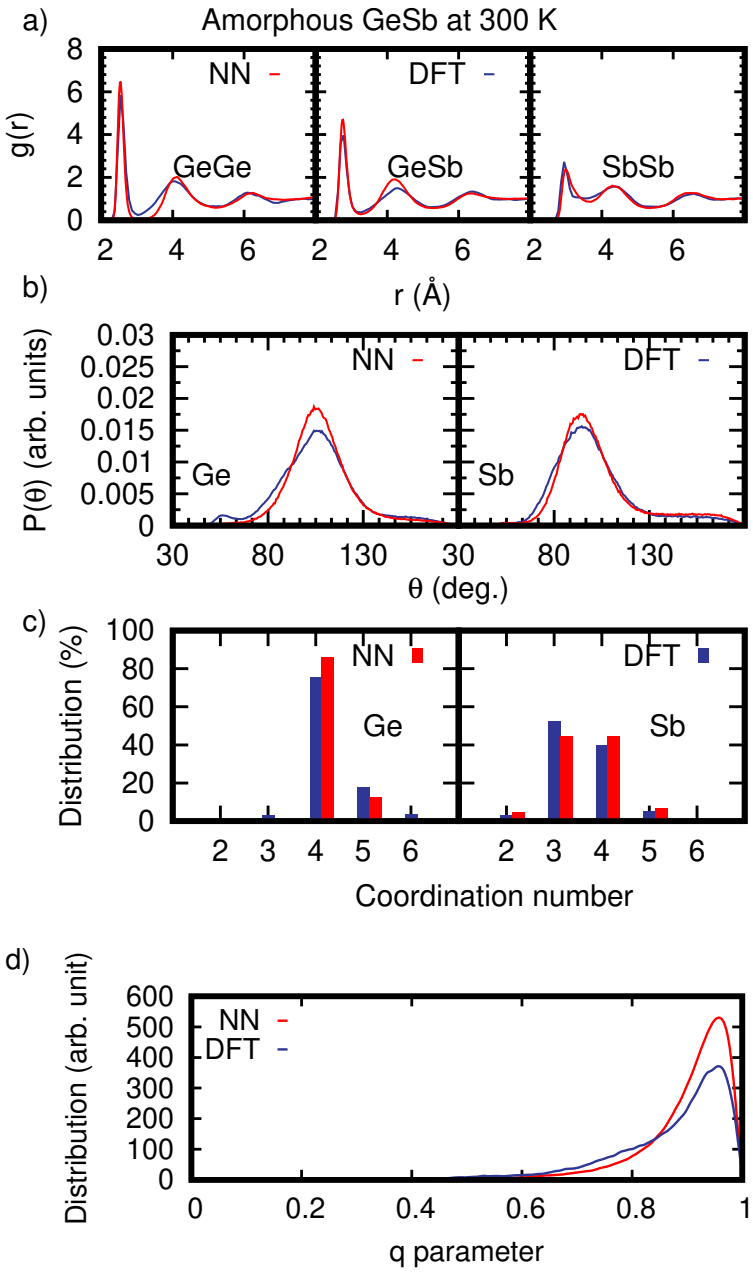

Figure S15: Structural properties of amorphous GeSb at 300 K from NN (red curves) and DFT (blue curves) simulations. NN (DFT) data refer to a 512-atom (148-atom) model. a) Total and partial radial distribution functions. b) Angular distribution function resolved per central atomic species. The data are normalized to the number of triplets in each model. c) Distribution of coordination numbers resolved per chemical species, obtained by integrating the pair correlation functions up to a bonding cutoff of 3.2 Å for all pairs. d) Distribution of the local order parameter q for tetrahedricity for four-coordinated Ge atoms.

Table S12: Average coordination numbers for different pairs of atoms in amorphous *GeSb* at 300 K generated from DFT (in parenthesis) and NN simulations. Details on the simulation cells and bonding cutoff are given in the caption of Fig. S15.

-	Ge	Sb
Total	4.13 (4.24)	3.53 (3.47)
With Ge	2.01 (2.27)	2.12 (1.97)
With Sb	2.12 (1.97)	1.41 (1.50)

2.6 $Ge_{15}Sb_{85}$

The structural properties of the liquid $Ge_{15}Sb_{85}$ at the experimental density of amorphous phase (0.0321 atoms/Å^3) [8] obtained from NN+D3 MD simulation with a 1000-atom model at 1000 K are compared with those obtained from DFT-MD simulation with a 200-atom model at the same density (see Fig. S16). The structural properties were averaged over a trajectory 50 ps long. The pair correlation functions, the bond angles distribution function and the distribution of coordination numbers are compared with DFT results in Fig. S16. Then we validated the NN potential on the structural properties of the amorphous phase at the same density. The 1000-atom liquid model was quenched from the melt at 1000 K to 300 K in 100 ps, and equilibrated at 300 K for 40 ps. Structural properties are averaged over a subsequent run 50 ps long. In Fig. S17, the structural properties from NN-MD are compared with those obtained from amorphous model generated with DFT-MD with similar protocol. The pair correlation functions, the bond angles distribution function, the distribution of coordination numbers and the distribution of the local order parameter q for tetrahedricity for four-coordinated Ge atom are compared with DFT results in Fig. S17. The average coordination number for different pairs of atoms are given in Table S13. We also quantified the fraction of four-coordinated Ge atoms in tetrahedral geometry by integrating the distribution of the q parameter between 0.8 and 1 as discussed previously, resulting in 81% in the NN model to be compared to the value of 53% in the DFT model. Similarly to other alloys, the structural properties of $Ge_{15}Sb_{85}$ obtained from NN-MD and DFT-MD simulations are in a good agreement. The largest misfit is in the fraction of Ge atoms in tetrahedral configuration which is overestimated in NN data. The large misfit in the Ge-Ge pair correlation function is due to the poor statistics in the small 200-atom cell for this composition with a low fraction of Ge.

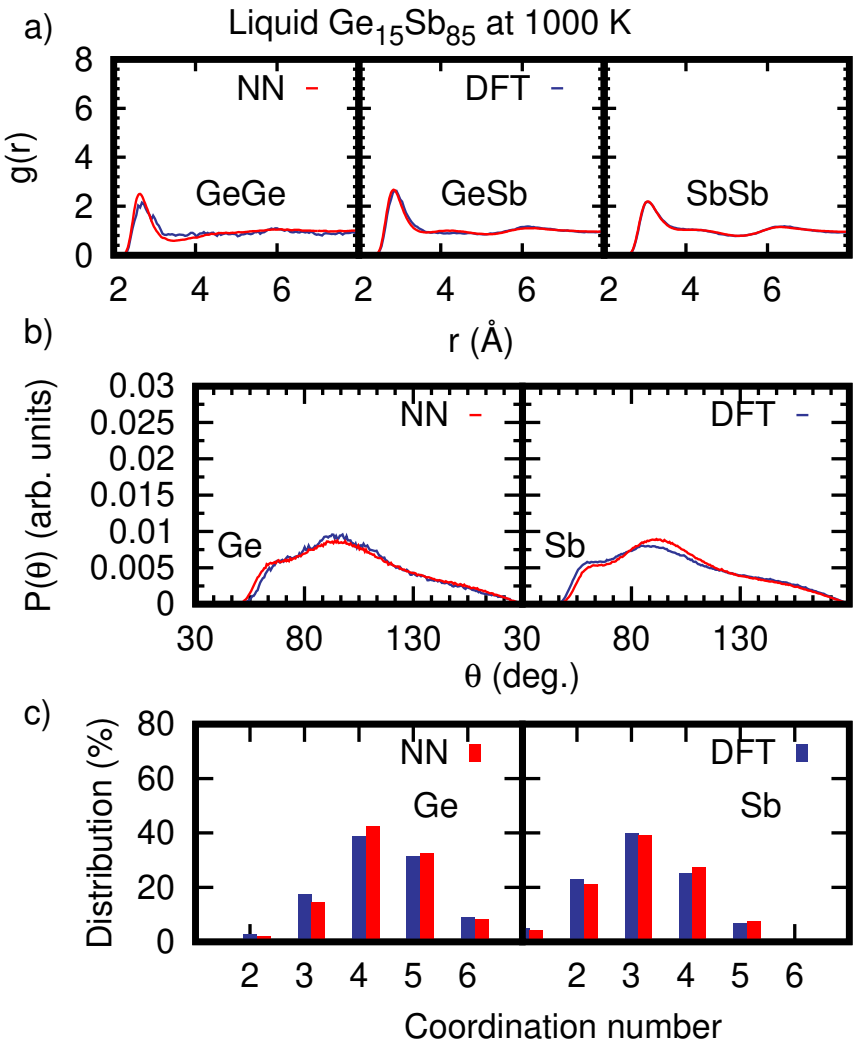

Figure S16: Structural properties of liquid $Ge_{15}Sb_{85}$ at 1000 K from NN (red curves) and DFT (blue curves) simulations. NN (DFT) data refer to a 1000-atom (200-atom) model. a) Total and partial radial distribution functions. b) Angular distribution function resolved per central atomic species. The data are normalized to the number of triplets in each model. c) Distribution of coordination numbers resolved per chemical species, obtained by integrating the pair correlation functions up to a bonding cutoff of 2.9 Å for Ge-Ge, 3.1 Å for Ge-Sb bonds and 3.5 Å for Sb-Sb. We used the same bonding cutoff of the amorphous phase.

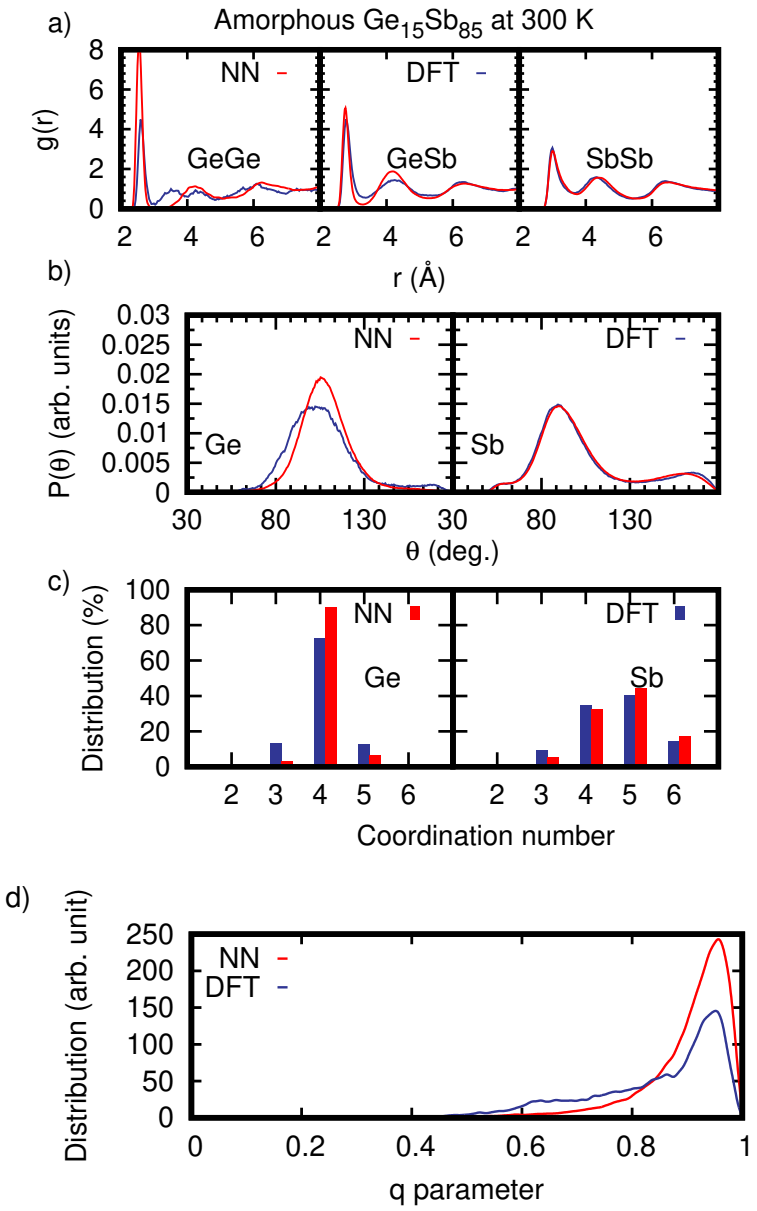

Figure S17: Structural properties of amorphous $Ge_{15}Sb_{85}$ at 300 K from NN (red curves) and DFT (blue curves) simulations. NN (DFT) data refer to a 1000-atom (200-atom) model. a) Total and partial radial distribution functions. b) Angular distribution function resolved per central atomic species. The data are normalized to the number of triplets in each model. c) Distribution of coordination numbers resolved per chemical species, obtained by integrating the pair correlation functions up to a bonding cutoff of 2.9 Å for Ge-Ge, 3.1 Å for Ge-Sb bonds and 3.5 Å for Sb-Sb. d) Distribution of the local order parameter q for tetrahedricity for four-coordinated Ge atoms.

Table S13: Average coordination numbers for different pairs of atoms in amorphous $Ge_{15}Sb_{85}$ at 300 K generated from DFT (in parenthesis) and NN simulations. Details on the simulation cells and bonding cutoff are given in the caption of Fig. S17.

-	Ge	Sb
Total	4.03 (3.97)	4.75 (4.63)
With Ge	0.73 (0.43)	0.58 (0.63)
With Sb	3.30 (3.54)	4.17 (4.00)

2.7 Sb_2Te_3

The structural properties of liquid Sb_2Te_3 at the experimental density of liquid phase (0.0281 atoms/Å^3 at 1003 K)[9] obtained from NN-MD simulation with a 960-atom model at 1000 K are compared with those obtained from DFT-MD simulation with a 200-atom model at the same density (see Fig. S18). The structural properties were averaged over a trajectory 50 ps long. The pair correlation functions, the bond angles distribution function and the distribution of coordination numbers are compared with DFT results in Fig. S18. Then, we validated the NN potential on the structural properties of the amorphous phase at the same density. The 960-atom liquid model was quenched from the melt at 1000 K to 300 K in 100 ps, and equilibrated at 300 K for 40 ps. Structural properties are averaged over a subsequent run 50 ps long. In Fig. S19, the structural properties from NN-MD are compared with those obtained from amorphous model generated by DFT-MD simulation with a similar protocol. The pair correlation functions, the bond angles distribution function, and the distribution of coordination numbers in Fig. S19. The average coordination number for different pairs of atoms are given in Table S14. Finally, the NN potential was validated on the structural properties of the trigonal crystal phase of Sb_2Te_3 by fitting the EOS (see Figs. S20). The resulting parameters at equilibrium are compared with DFT data in Tables S15. Overall, the structural properties of Sb_2Te_3 from NN-MD simulations are in a good agreement with those obtained from DFT-MD. The largest misfit is in the EOS of the trigonal phase with a 4 meV/atom error on the equilibrium energy, which is still comparable to the average error of the NN potential. In particular, the NN potential overestimates the formation energy of the trigonal phase. This misfit would further favor the formation of the trigonal phase in the decomposition of alloys along the Ge-Sb_2Te_3 tie-line. Therefore, the fact that this phase does not form in our MD simulations (see Sec. 4 of the article) is a genuine kinetic effect and can not be ascribed to errors in the NN formation energy of the crystalline products.

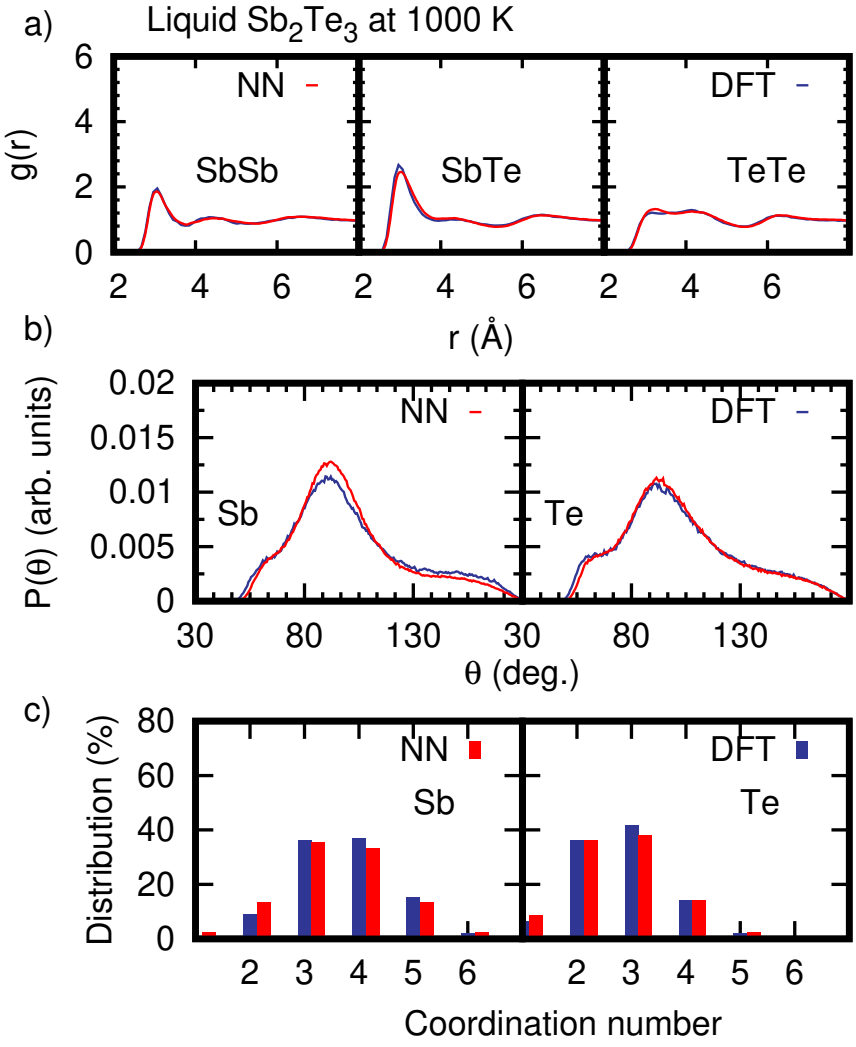

Figure S18: Structural properties of liquid Sb_2Te_3 at 1000 K from NN (red curves) and DFT (blue curves) simulations. NN (DFT) data refer to a 960-atom (200-atom) model. a) Total and partial radial distribution functions. b) Angular distribution function resolved per central atomic species. The data are normalized to the number of triplets in each model. c) Distribution of coordination numbers resolved per chemical species, obtained by integrating the pair correlation functions up to a bonding cutoff of 3.2 Å for Sb-Sb and Te-Te and of 3.4 Å for Sb-Te. We used the same bonding cutoff of the amorphous phase.

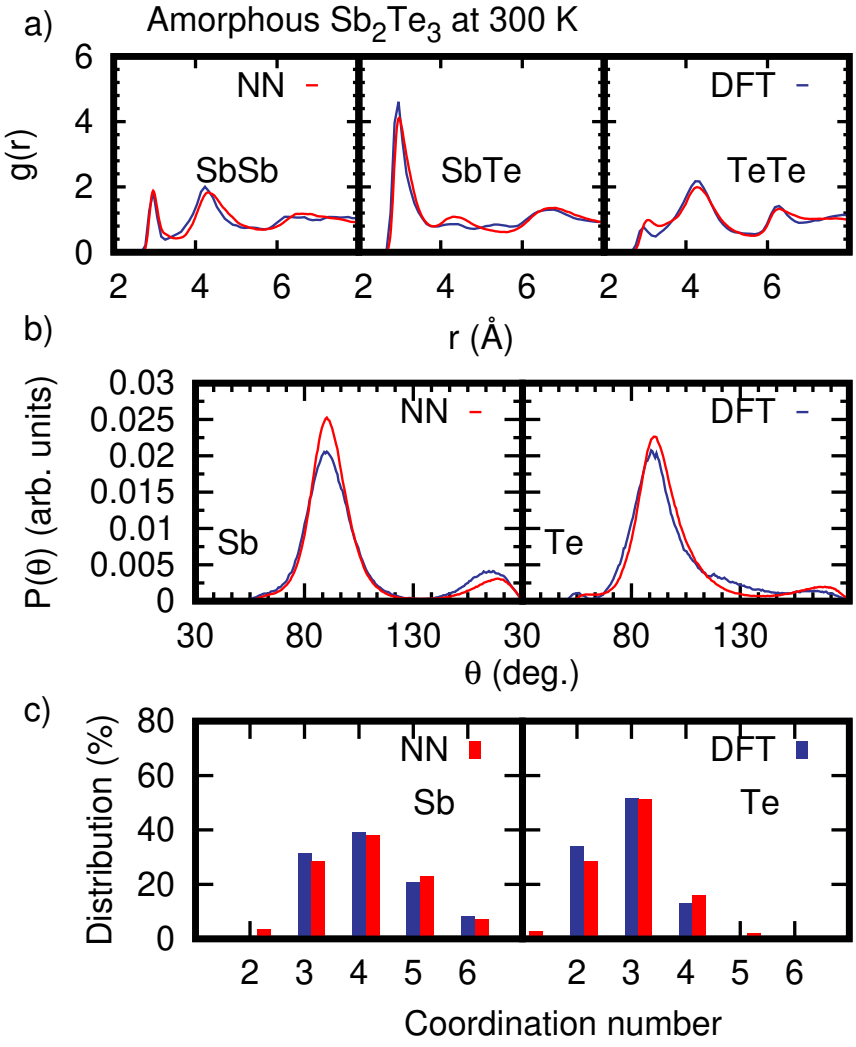

Figure S19: Structural properties of amorphous Sb_2Te_3 at 300 K from NN (red curves) and DFT (blue curves) simulations. NN (DFT) data refer to a 960-atom (200-atom) model. a) Total and partial radial distribution functions. b) Angular distribution function resolved per central atomic species. The data are normalized to the number of triplets in each model. c) Distribution of coordination numbers resolved per chemical species, obtained by integrating the pair correlation functions up to a bonding cutoff of 3.2 Å for Sb-Sb and Te-Te and of 3.4 Å for Sb-Te.

Table S14: Average coordination numbers for different pairs of atoms in amorphous Sb_2Te_3 at 300 K generated from DFT (in parenthesis) and NN simulations. Details on the simulation cells and bonding cutoff are given in the caption of Fig. S19.

-	Sb	Te
Total	4.02 (4.05)	2.85 (2.80)
With Sb	0.59 (0.56)	2.28 (2.32)
With Te	3.42 (3.48)	0.57 (0.48)

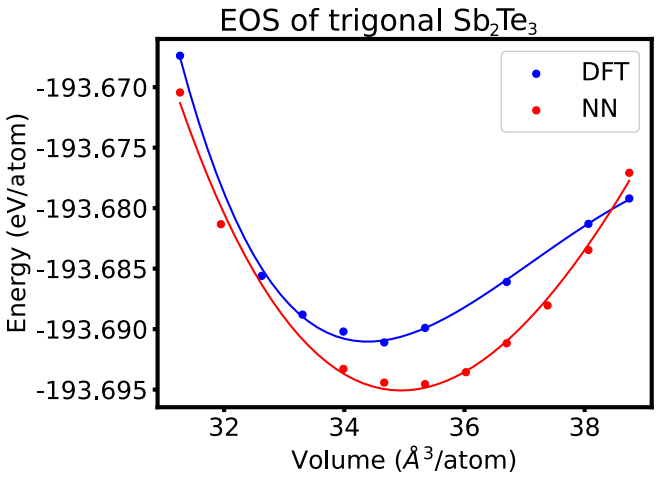

Figure S20: Equation of state (EOS) of the trigonal phase of Sb_2Te_3 from DFT and NN calculations.

Table S15: Fitting parameters of the Birch-Murnaghan equation of state of the trigonal phase of Sb_2Te_3 from NN and DFT-PBE calculations at zero temperature. The energy (E_0), volume (V_0), bulk modulus (B) and derivative of B (B') at equilibrium are reported.

	E_0 (eV atom^{-1})	V_0 (Å^3 atom^{-1})	B (GPa)	B'
DFT	-193.691	34.40	16.15	16.5
NN	-193.695	34.94	16.05	4.3

2.8 Sb_2Te

The structural properties of liquid Sb_2Te at the experimental density of amorphous phase (0.0309 atoms/Å^3)[10] obtained from NN-MD simulation with a 1152-atom model at 1000 K are compared with those obtained from DFT-MD simulation with a 198-atom model at the same density (see Fig. S21). The structural properties were averaged over a trajectory 50 ps long. The pair correlation functions, the bond angles distribution function and the distribution of coordination numbers are compared with DFT results in Fig. S21. Then we validated the NN potential on the structural properties of the amorphous phase at the same density. The 1152-atom liquid model was quenched from the melt at 1000 K to 300 K in 100 ps, and equilibrated at 300 for 40 ps. Structural properties were averaged over a subsequent run 50 ps long. In Fig. S22, the structural properties from NN-MD are compared with those obtained from amorphous model generated with DFT-MD simulation with similar protocol. The pair correlation functions, the bond angles distribution function, and the distribution of coordination numbers in Fig. S22. The average coordination number for different pairs of atoms are given in Table S16.

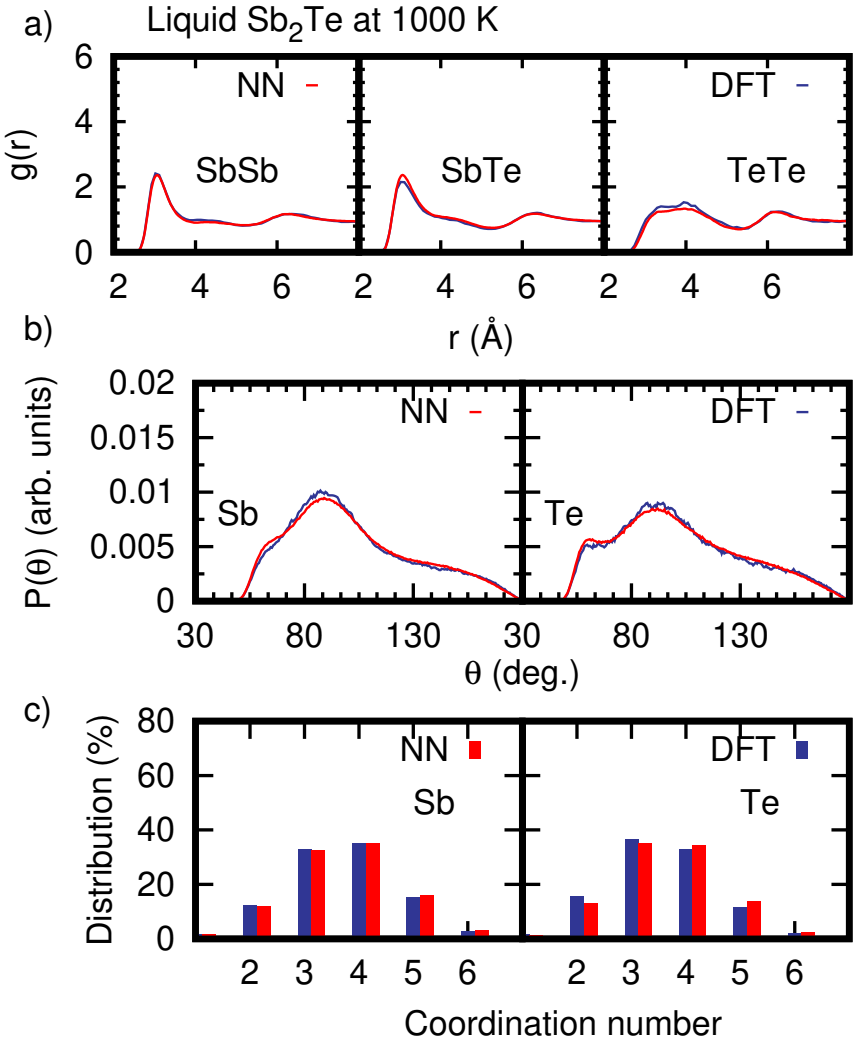

Figure S21: Structural properties of liquid Sb_2Te at 1000 K from NN (red curves) and DFT (blue curves) simulations. NN (DFT) data refer to a 1152-atom (198-atom) model. a) Total and partial radial distribution functions. b) Angular distribution function resolved per central atomic species. The data are normalized to the number of triplets in each model. c) Distribution of coordination numbers resolved per chemical species, obtained by integrating the pair correlation functions up to a bonding cutoff of 3.2 Å for Sb-Sb and Te-Te and of 3.4 Å for Sb-Te. We used the same bonding cutoff of the amorphous phase.

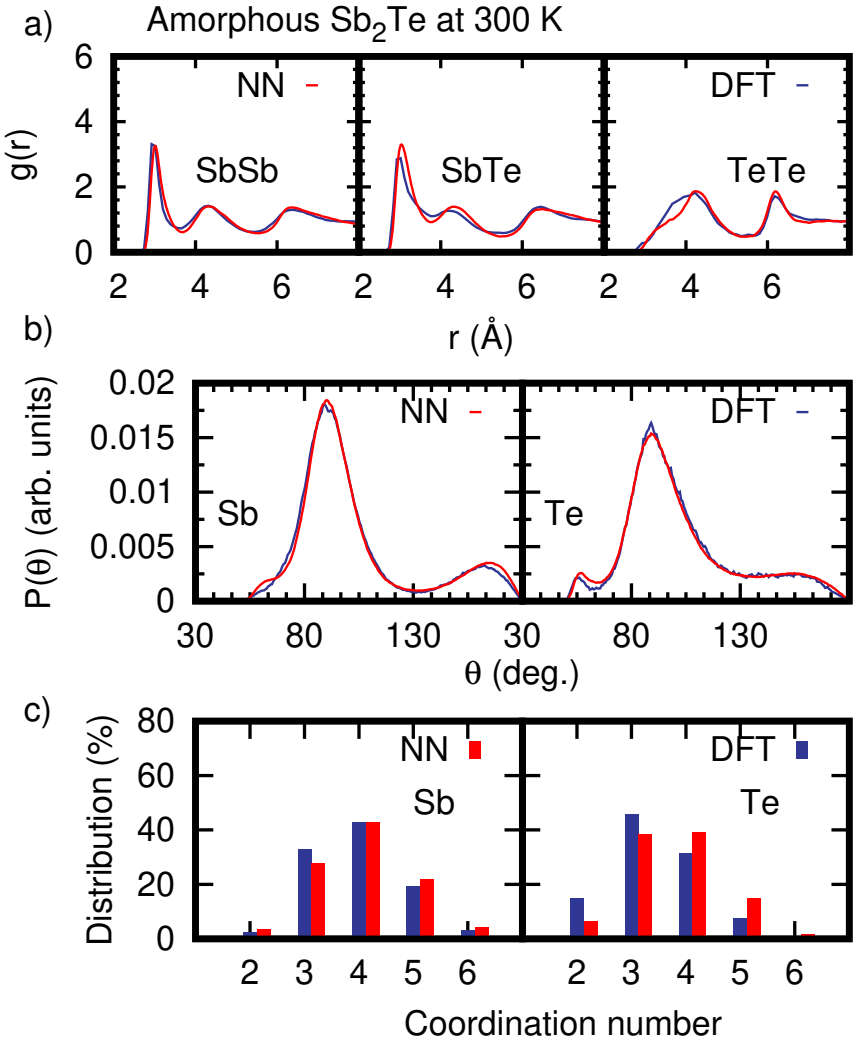

Figure S22: Structural properties of amorphous Sb_2Te at 300 K from NN (red curves) and DFT (blue curves) simulations. NN (DFT) data refer to a 1152-atom (198-atom) model. a) Total and partial radial distribution functions. b) Angular distribution function resolved per central atomic species. The data are normalized to the number of triplets in each model. c) Distribution of coordination numbers resolved per chemical species, obtained by integrating the pair correlation functions up to a bonding cutoff of 3.2 Å for Sb-Sb and Te-Te and of 3.4 Å for Sb-Te.

Table S16: Average coordination numbers for different pairs of atoms in amorphous Sb_2Te at 300 K generated from DFT (in parenthesis) and NN simulations. Details on the simulation cells and bonding cutoff are given in the caption of Fig. S22.

-	Sb	Te
Total	3.95 (3.88)	3.67 (3.32)
With Sb	2.17 (2.29)	3.55 (3.17)
With Te	1.78 (1.59)	0.11 (0.15)

2.9 *Ge*

The structural properties of liquid Ge at the experimental density of the amorphous phase (0.0438 atoms/Å^3)[11] obtained from NN-MD simulation with a 2400-atom model at 1250 K are compared with those obtained from DFT-MD simulation with a 300-atom model from Ref. [1] at the same density (see Fig. S23). The structural properties were averaged over a trajectory 50 ps long. The pair correlation functions, the bond angles distribution function and the distribution of coordination numbers are compared with DFT results in Fig. S23. Then we validated the NN potential on the structural properties of the amorphous phase at the same density. The 2400-atom liquid model was quenched from the melt at 1250 K to 300 K in 100 ps, and then equilibrated at 300 K for 40 ps. Structural properties are averaged over a subsequent 50 ps long. In Fig. S24, the structural properties from NN-MD are compared with those obtained from an amorphous model generated by DFT-MD simulation in Ref. [1] with a similar protocol. The pair correlation functions, the bond angles distribution function, the distribution of coordination numbers and the distribution of the local order parameter q for tetrahedricity for four-coordinated Ge atom are compared with DFT results in Fig. S24. We also quantified the fraction of four-coordinated Ge atoms in tetrahedral geometry by integrating the distribution of q by integrating the q parameter between 0.8 and 1 as discussed in previously, resulting in 64% in NN model compared to 68% in DFT results from Ref. [1]. Finally, the NN potential was validated on the structural properties of the diamond crystal phase of Ge by fitting the EOS (see Figs. S25). The resulting parameters at equilibrium are compared with DFT data in Tables S17.

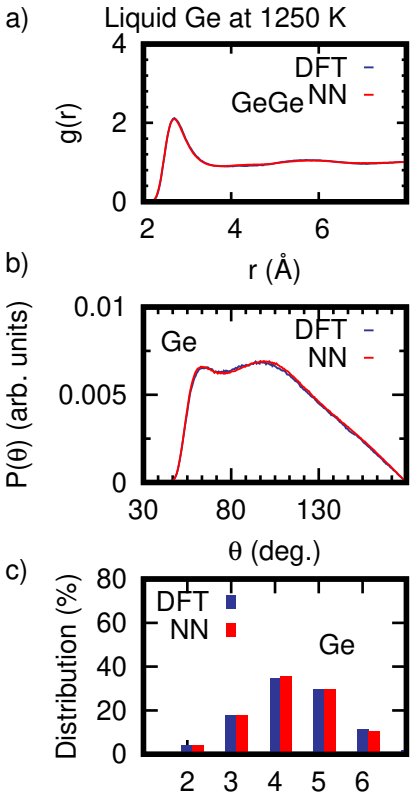

Figure S23: Structural properties of liquid Ge at 1250 K from NN (red curves) and DFT (blue curves) simulations. NN (DFT) data refer to a 2400-atom (300-atom) model. a) Total radial distribution functions. b) Angular distribution function resolved per central atomic species. The data are normalized to the number of triplets in each model. c) Distribution of coordination numbers resolved per chemical species, obtained by integrating the pair correlation functions up to a bonding cutoff of 3.0 Å. We used the same bonding cutoff of the amorphous phase.

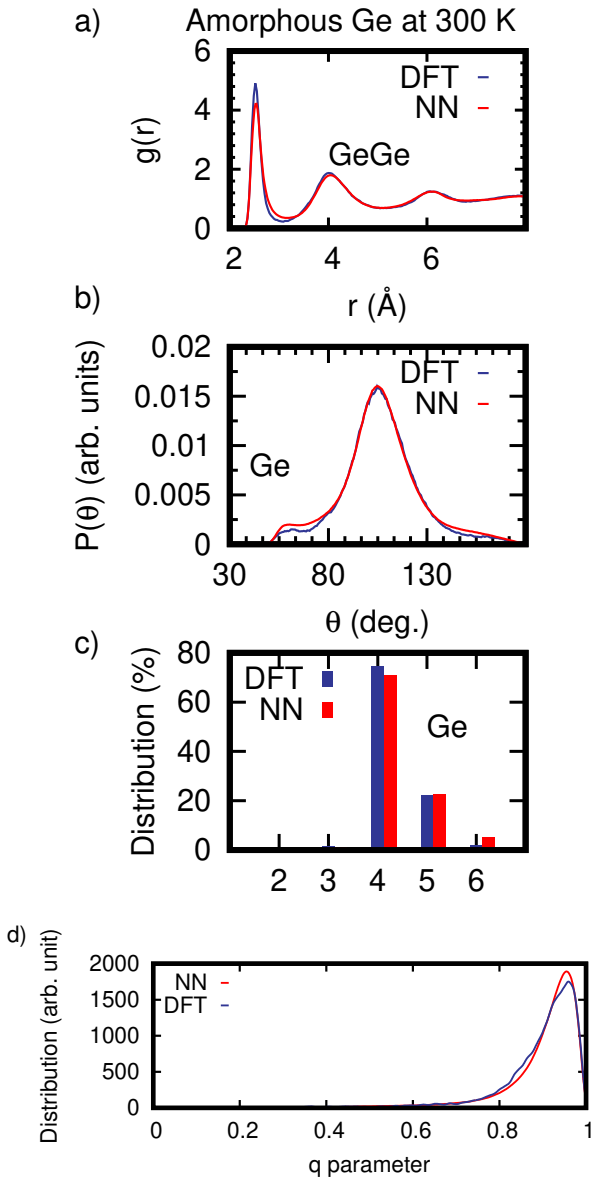

Figure S24: Structural properties of amorphous Ge at 300 K from NN (red curves) and DFT (blue curves) simulations. NN (DFT) data refer to a 2400-atom (300-atom) model. a) Total radial distribution functions. b) Angular distribution function resolved per central atomic species. The data are normalized to the number of triplets in each model. c) Distribution of coordination numbers resolved per chemical species, obtained by integrating the pair correlation functions up to a bonding cutoff of 3.0 Å. d) Distribution of the local order parameter q for tetrahedricity for four-coordinated Ge atoms.

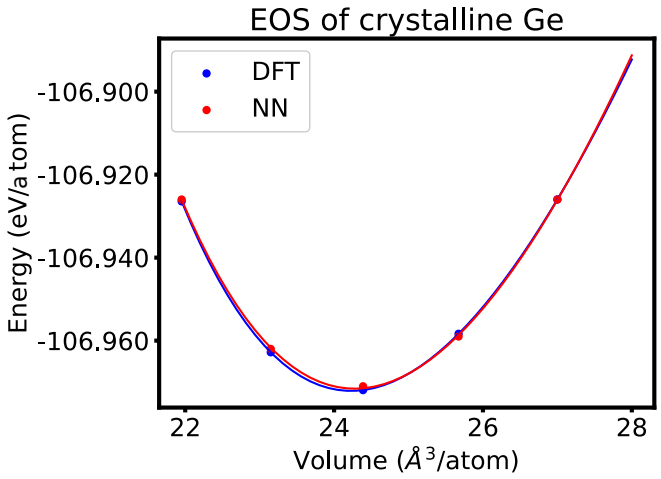

Figure S25: Equation of state (EOS) of the crystalline phase of Ge from DFT and NN calculations.

Table S17: Fitting parameters of the Birch-Murnaghan equation of state of crystalline Ge from NN and DFT-PBE calculations at zero temperature. The energy (E_0), volume (V_0), bulk modulus (B) and derivative of B (B') at equilibrium are reported.

	E_0 (eV atom^{-1})	V_0 (Å^3 atom^{-1})	B (GPa)	B'
DFT	-106.972	24.22	57.58	4.64
NN	-106.972	24.27	56.20	3.60

2.10 *Sb*

The structural properties of liquid Sb at the experimental density at melting (0.0320 atoms/Å^3)[12] obtained from NN-MD simulation with a 1000-atom model at 1000 K and compared with those obtained from DFT-MD simulation with a 144-atom model from Ref. [13] at the same density (see Fig. S26). The structural properties were averaged over a trajectory 50 ps long. The pair correlation functions, the bond angles distribution function and the distribution of coordination numbers are compared with DFT results in Fig. S26. Then, we validated the NN potential on the structural properties of the amorphous phase at the same density. The 1000-atom liquid model was quenched from the melt at 1000 K to 300 K in 100 ps, and equilibrated at 300 K for 40 ps. Structural properties are averaged over a subsequent run 50 ps long. In Fig. S27, structural properties from NN-MD are compared with those obtained from an amorphous model generated by DFT-MD simulation in Ref. [13] with a similar protocol. The pair correlation functions, the bond angles distribution function, and the distribution of coordination numbers. Finally, the NN potential was validated on

the structural properties of the trigonal crystal phase of Sb by fitting the EOS (see Figs. S28). The resulting parameters at equilibrium are compared with DFT data in Tables S18.

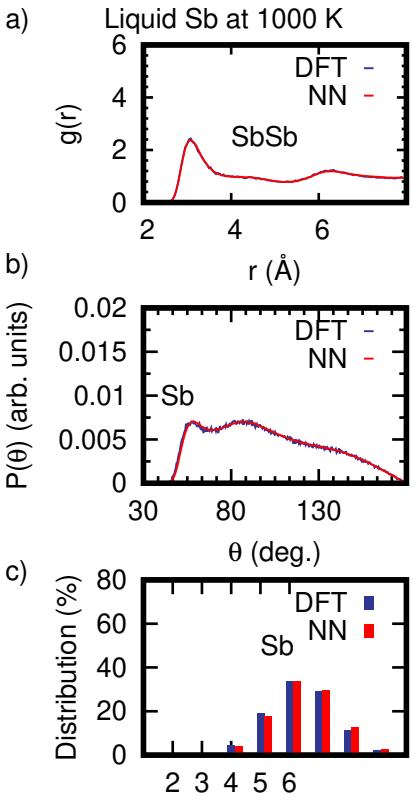

Figure S26: Structural properties of liquid Sb at 1000 K from NN (red curves) and DFT (blue curves) simulations. NN (DFT) data refer to a 1000-atom (144-atom) model. a) Total and partial radial distribution functions. b) Angular distribution function resolved per central atomic species. The data are normalized to the number of triplets in each model. c) Distribution of coordination numbers resolved per chemical species, obtained by integrating the pair correlation functions up to a bonding cutoff of 3.66 Å. We used the same bonding cutoff of the amorphous phase.

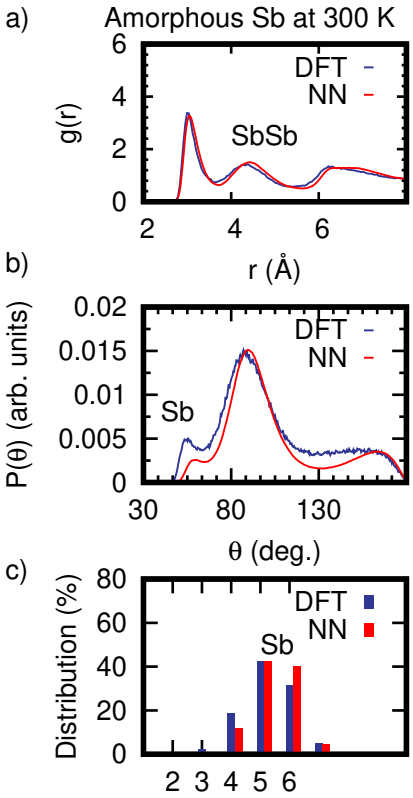

Figure S27: Structural properties of amorphous Sb at 300 K from NN (red curves) and DFT (blue curves) simulations. NN (DFT) data refer to a 1000-atom (144-atom) model. a) Total and partial radial distribution functions. b) Angular distribution function resolved per central atomic species. The data are normalized to the number of triplets in each model. c) Distribution of coordination numbers resolved per chemical species, obtained by integrating the pair correlation functions up to a bonding cutoff corresponding of 3.5 Å.

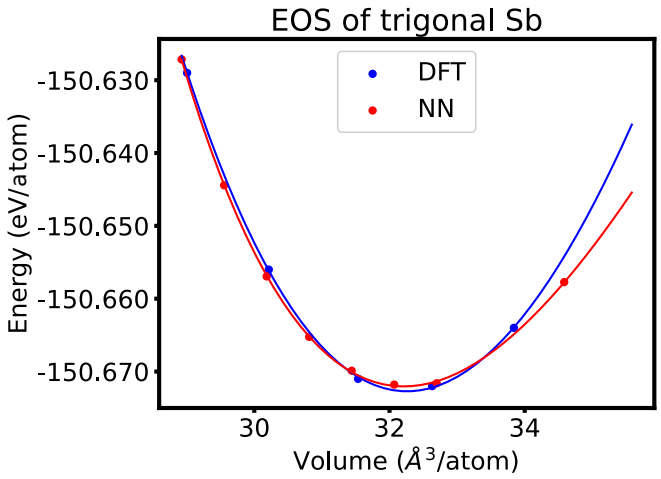

Figure S28: Equation of state (EOS) of the trigonal phase of Sb from DFT and NN calculations.

Table S18: Fitting parameters of the Birch-Murnaghan equation of state of hexagonal Sb from NN and DFT-PBE calculations at zero temperature. The energy (E_0), volume (V_0), bulk modulus (B) and derivative of B (B') at equilibrium are reported.

	E_0 (eV atom^{-1})	V_0 (Å^3 atom^{-1})	B (GPa)	B'
DFT	-150.673	32.26	38.2	2.3
NN	-150.672	32.21	31.9	7.3

2.11 *Te*

The structural properties of the liquid Te at the experimental density at melting (0.0268 atoms/Å^3) [14] obtained from NN-MD simulation with a 1000-atom model at 1000 K and compared with those obtained from DFT-MD simulation with a 200-atom model at the same density (see Fig. S29). The structural properties were averaged over a trajectory 50 ps long. The pair correlation functions, the bond angles distribution function and the distribution of coordination numbers are compared with DFT results in Fig. S29. Finally, the NN potential was validated on the structural properties of the crystalline phase of Te by fitting the EOS (see Figs. S30). The resulting parameters at equilibrium are compared with DFT data in Tables S19.

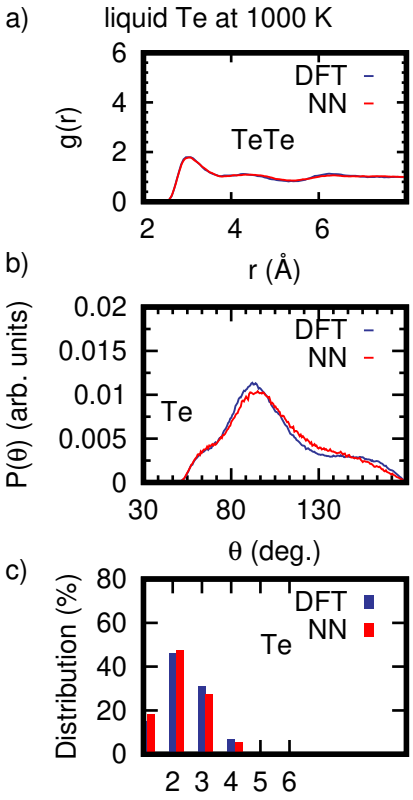

Figure S29: Structural properties of liquid Te at 1000 K from NN (red curves) and DFT (blue curves) simulations. NN (DFT) data refer to a 1000-atom (200-atom) model. Total and partial radial distribution functions. b Angular distribution function resolved per central atomic species. The data are normalized to the number of triplets in each model. c) Distribution of coordination numbers resolved per chemical species, obtained by integrating the pair correlation functions up to a bonding cutoff of 3.2 Å.

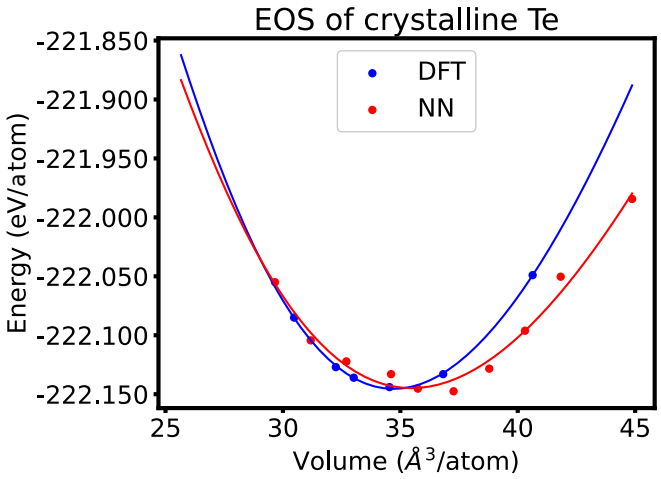

Figure S30: Equation of state (EOS) of the crystalline phase of Te from DFT and NN calculations.

Table S19: Fitting parameters of the Birch-Murnaghan equation of state of the crystalline phase of Te from NN and DFT-PBE calculations at zero temperature. The energy (E_0), volume (V_0), bulk modulus (B) and derivative of B (B') at equilibrium are reported.

	E_0 (eV atom^{-1})	V_0 (Å^3 atom^{-1})	B (GPa)	B'
DFT	-222.145	34.71	34.6	1.1
NN	-222.145	35.47	26.5	1.4

3 Transferability

Beside describing the structural properties of GeSbTe alloys included in the training set, we have tested the transferability of the MLIP to alloys outside the training set. Hereafter, we report the structural properties of the GST725 and $Ge_{9.\bar{6}}Sb_2Te_5$ alloys whose crystallization kinetics was addressed by NN-MD simulations in the article, and two other alloys along the Ge-Sb_2Te_3 tie-line.

3.1 $Ge_7Sb_2Te_5$

In the lack of experimental data for the density of $Ge_7Sb_2Te_5$, we have modeled this alloy in a 1008-atom cubic cell at the theoretical density of the liquid at 1000 K of 0.0335 atom/Å^3, obtained from a DFT+D3 NPT simulation with the NN potential. The liquid model was quenched from the melt at 1000 K to 300 K in 100 ps, and equilibrated at 300 K for 40 ps. Structural properties are averaged over a subsequent run 50 ps long. The structural properties of the amorphous phase are compared with those obtained from DFT-MD simulation with a 200-atom model in Fig. S31, including the pair correlation functions, the bond angles distribution function, the distribution of coordination numbers and the distribution of the local order parameter q for tetrahedricity for four-coordinated Ge atom. The average coordination number for different pairs of atoms are given in Table S20. The fraction of Ge atoms in tetrahedral geometry is 42% in the NN model to be compared with the value of 45% in the DFT model.

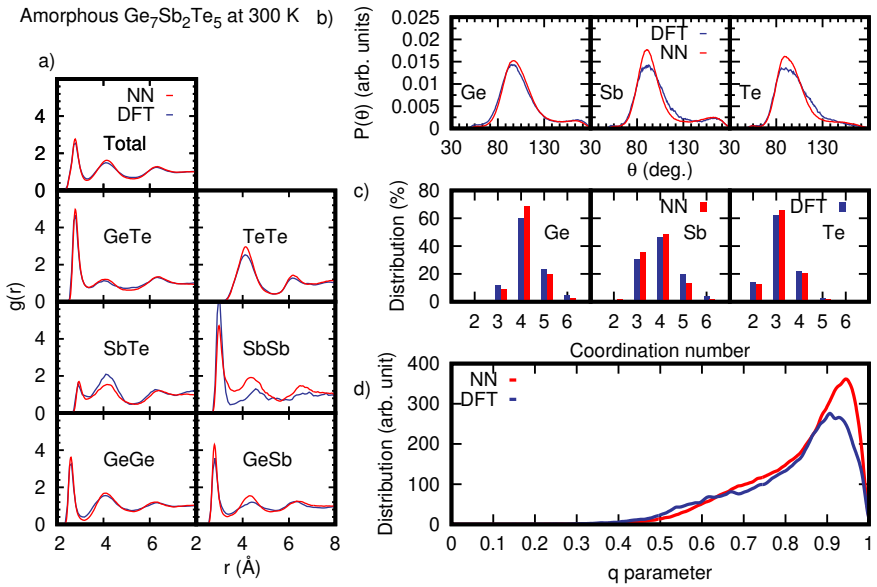

Figure S31: Structural properties of amorphous GST725 at 300 K from NN (red curves) and DFT (blue curves) simulations. NN (DFT) data refer to a 1008-atom (210-atom) model. a) Total and partial radial distribution functions. b) Angular distribution function resolved per central atomic species. The data are normalized to the number of triplets in each model. c) Distribution of coordination numbers resolved per chemical species, obtained by integrating the pair correlation functions up to a bonding cutoff corresponding to 3.2 Å for all pairs except for Sb-Te for which a longer cutoff of 3.4Å was used. d) Distribution of the local order parameter q for tetrahedricity for four-coordinated Ge atoms.

The fraction of Ge atoms in tetrahedral geometry is 46% in the NN model to be compared with the value of 40% in the DFT model.

Table S20: Average coordination numbers for different pairs of atoms in amorphous GST725 at 300 K generated from DFT (in parenthesis) and NN simulations. Details on the simulation cells and bonding cutoff are given in the caption of Fig. S31.

-	Ge	Sb	Te
Total	4.15 (4.20)	3.77 (3.95)	3.11 (3.12)
With Ge	1.60 (1.68)	2.09 (2.00)	2.73 (2.72)
With Sb	0.60 (0.57)	0.72 (0.97)	0.38 (0.39)
With Te	1.95 (1.94)	0.95 (0.98)	0.00 (0.00)

3.2 $Ge_{9.\bar{6}}Sb_2Te_5$

In the lack of experimental data on $Ge_{9.\bar{6}}Sb_2Te_5$, we have modeled this alloy in a 1000-atom cubic cell at the theoretical density of 0.0359 atom/Å^3. This density was obtained from a NPT simulation with the NN+D2 potential in the liquid at 1000 K. The initial density for this simulation was linearly extrapolated from the density of amorphous Ge and GST725 (0.0382 atom/Å^3). After an equilibration MD simulation 30 ps long, we obtained the theoretical density of 0.0359 atom/Å^3 as the average over 30 ps. This value is slightly lower than the initial estimate. The liquid model was quenched from the melt at 1000 K to 300 K in 100 ps, and equilibrated at 300 K for 40 ps. Structural properties are averaged over a subsequent run 50 ps long.

The structural properties of the amorphous phase from NN-MD simulation are compared with those obtained from DFT-MD simulation with a 200-atom model in Fig. S32, including the pair correlation functions, the bond angles distribution function, the distribution of coordination numbers and the distribution of the local order parameter q for tetrahedricity for four-coordinated Ge atom. The average coordination number for different pairs of atoms are given in Table S21. The fraction of Ge atoms in tetrahedral geometry is 46% in the NN model to be compared with the value of 39% in the DFT model.

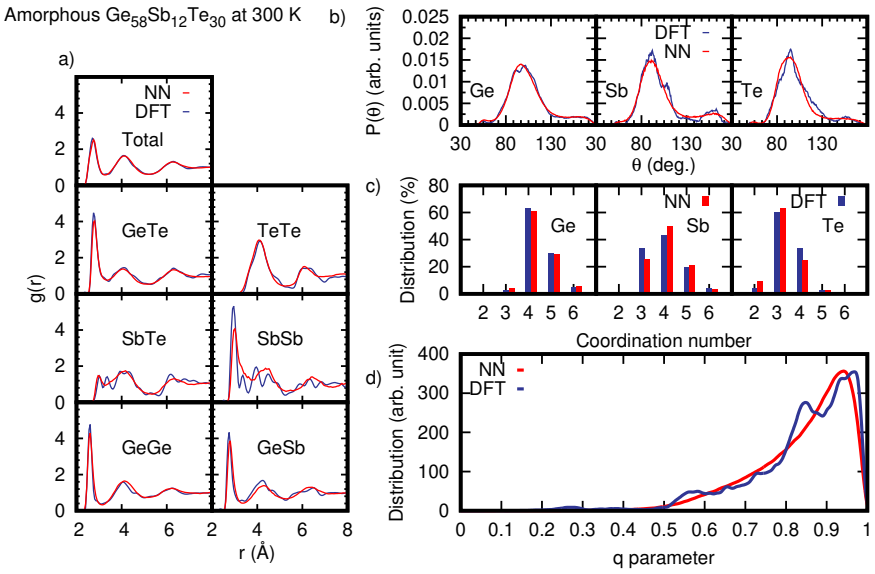

Figure S32: Structural properties of amorphous $Ge_{9.\bar{6}}Sb_2Te_5$ ($Ge_{58}Sb_{12}Te_{30}$) at 300 K from NN (red curves) and DFT (blue curves) simulations. NN (DFT) data refer to a 1000-atom (210-atom) model. a) Total and partial radial distribution functions. b Angular distribution function resolved per central atomic species. The data are normalized to the number of triplets in each model. c Distribution of coordination numbers resolved per chemical species, obtained by integrating the pair correlation functions up to a bonding cutoff of 3.2 Å for all pairs except for Sb-Te for which a longer cutoff of 3.4 Å was used. d) Distribution of the local order parameter q for tetrahedricity for four-coordinated Ge atoms.

Table S21: Average coordination numbers for different pairs of atoms in amorphous $Ge_{9.\bar{6}}Sb_2Te_5$ at 300 K generated from DFT (in parenthesis) and NN simulations. Details on the simulation cells and bonding cutoff are given in the caption of Fig. S32.

-	Ge	Sb	Te
Total	4.38 (4.36)	4.01 (3.94)	3.21 (3.12)
With Ge	2.39 (2.29)	2.49 (2.44)	2.85 (2.72)
With Sb	0.52 (0.51)	0.63 (0.69)	0.35 (0.39)
With Te	1.47 (1.56)	0.89 (0.81)	0.01 (0.00)

3.3 Alloys along the Ge-Sb_2Te_3 tie-line

As a final test on the transferability of the NN potential, in this section we report on the structural properties of alloys along the Ge-Sb_2Te_3 tie-line which were

investigated by DFT+D3 simulation in Ref. [6]. Here, we compare the NN+D3 and DFT+D3 following the same protocol used in Ref. [6] to generate amorphous models of GST423 (see Fig. S33) and GST323 (see Fig. S34).

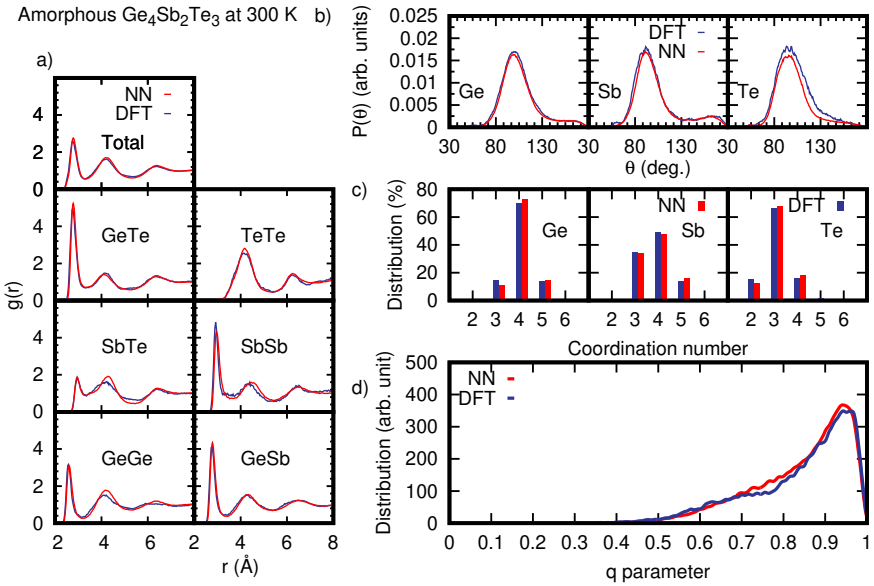

Figure S33: Structural properties of amorphous GST423 at 300 K from NN+D3 (red curves) and DFT+D3 (blue curves) simulations. NN (DFT) data refer to a 864-atom (216-atom) model. a) Total and partial radial distribution functions. b) Angular distribution function resolved per central atomic species. The data are normalized to the number of triplets in each model. c) Distribution of coordination numbers resolved per chemical species, obtained by integrating the pair correlation functions up to a bonding cutoff of 3.2 Å for all pairs except for Sb-Te for which a longer cutoff of 3.4 Å was used. d) Distribution of the local order parameter q for tetrahedricity for four-coordinated Ge atoms for the NN model.

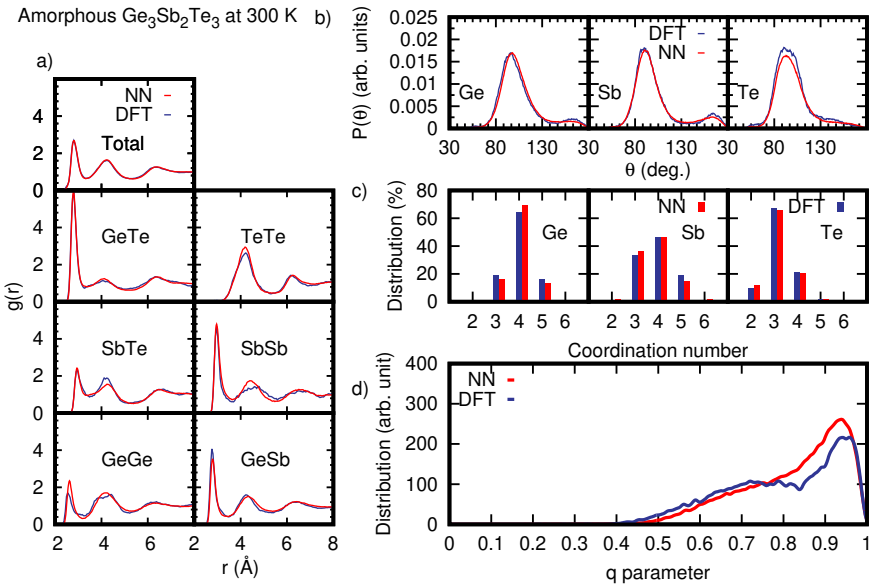

Figure S34: Structural properties of amorphous GST323 at 300 K from NN+D3 (red curves) and DFT+D3 (blue curves) simulations. NN (DFT) data refer to a 864-atom (216-atom) model. a) Total and partial radial distribution functions. b) Angular distribution function resolved per central atomic species. The data are normalized to the number of triplets in each model. c) Distribution of coordination numbers resolved per chemical species, obtained by integrating the pair correlation functions up to a bonding cutoff of 3.2 Å for all pairs except for Sb-Te for which a longer cutoff of 3.4Å was used. d) Distribution of the local order parameter q for tetrahedricity for four-coordinated Ge atoms.

4 Crystallization of Ge-Sb-Te alloys

4.1 Crystallization of GST225

Before investigating the crystallization with phase separation in GGST alloys, we first validated the NN potential on the crystallization of GST225 by computing the crystal growth velocity in the supercooled liquid. To this aim, we used 12960-atom model of the cubic-liquid interface from Ref. [3] to simulate heterogeneous crystallization. The crystal-liquid interface in our model corresponds to the (001) surface of the cubic crystal. We performed several independent constant volume simulations in the range 500–875 K. The potential energy as a function of time is reported in Fig. S35, from which we can se that the melting temperature is 872 K, close to the experimental value of 900 K [15]. From these simulation we estimated the crystal growth velocity $v_g = \frac{dL(t)}{dt}$, where $L(t)$ is the effective thickness of the crystalline region is given by

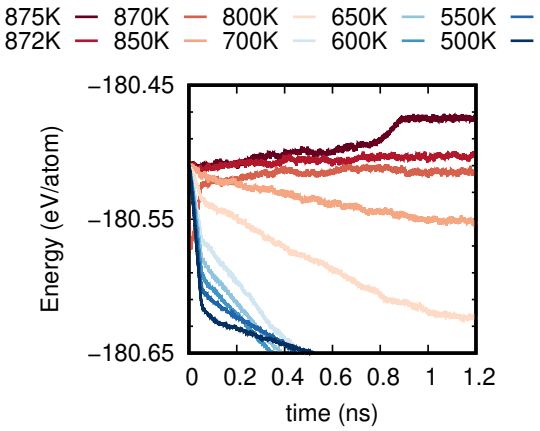

Figure S35: The potential energy as a function of time at different temperatures of the cubic-liquid interface model of GST225. At 875 K the raise in the potential energy is due to the melting of the crystalline slab, while in the range 870-872 K the system reach a plateau suggesting to be very close to the melting temperature.

$L(t) = N(t)/2A\rho$. A is the cross section of the simulation cell and the factor two takes into account the presence of two growing surfaces. From the time evolution of L(t) we can extract the v_g by as the slope of the linear region (see Fig. S36). The result on v_g are given in Fig. 3 in the article.

4.2 Crystallization with phase separation of GST725

We simulated the crystallization and phase separation of GST725 with a 8064-atom cell at the theoretical density of the liquid phase at 1000 K estimated form DFT-NPT simulation (0.0335 atom/Å^3). By assuming that GST725 will decompose into the thermodynamically favored products (Ge and GST225), and that Ge will segregate into the amorphous phase at its equilibrium density, the density of the remaining GST225 of 0.0296 atom/Å^3 is 4% lower than the equilibrium density of amorphous GST225 (0.0309 atom/Å^3). We started from a model equilibrated at 1400 K for 20 ps, followed by a second equilibration at 1000 K for 20 ps, and a rapid quenching to 600 K in 40 ps. Once we reached the target temperature, we simulated the crystallization with phase separation for about 7 ns at NVT conditions. The cluster analysis (see Sec. II in the article) yielded the same environments identified in GST523 (see Table I in the article), but for interfacial Te atoms that were not found in this latter alloy.

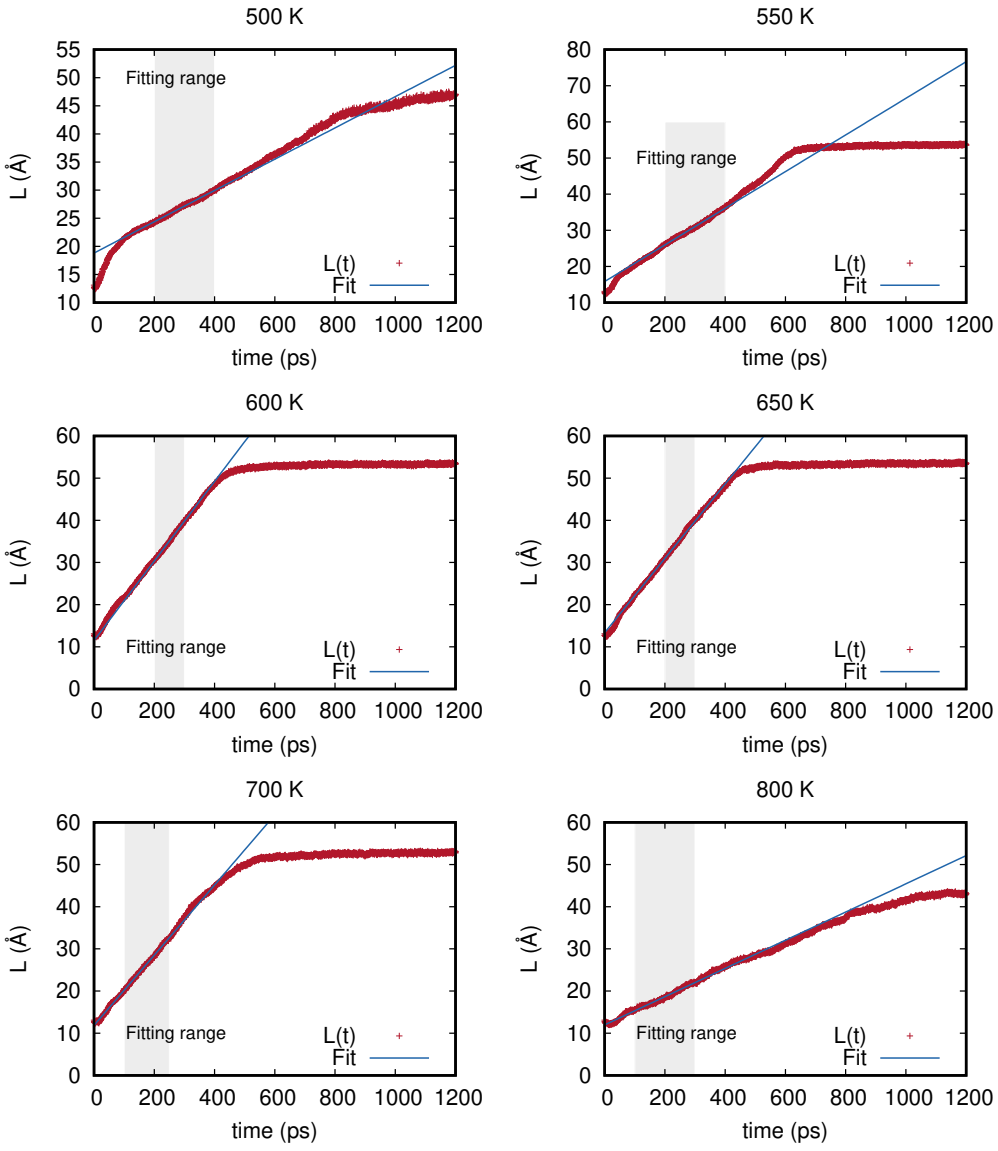

Figure S36: The evolution of the the effective (half) thickness of the crystalline slab $L(t)$ in simulations of GST225 at different temperatures and their linear fit in the range highlighted in gray which yields the crystal growth velocity.

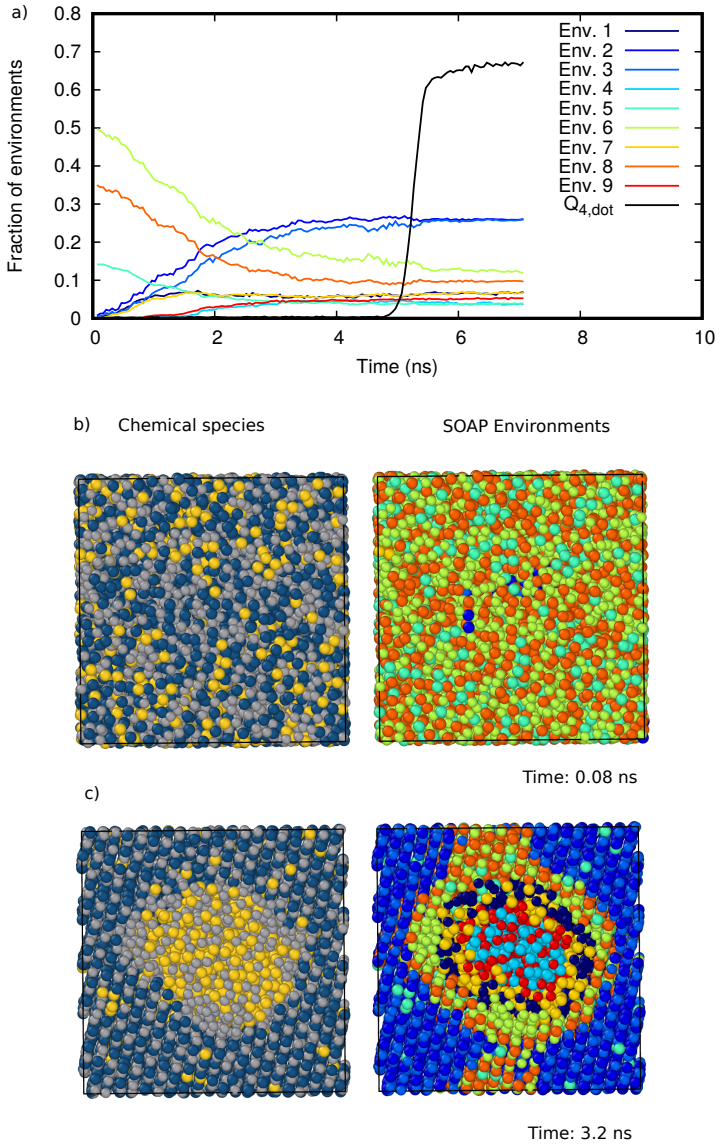

Figure S37: Evolution in time of the fraction of atoms in the ten different SOAP environments during the crystallization of GST725. The description of the different environments is given in Table I in the article. Snapshot of the transformation process at b) the beginning and c) at the end of the simulation. In the panels on the left atoms are colored according to the chemical species (Ge, Sb, Te in gray, yellow and blue). In the panels on the right, atoms are colored according to the different SOAP environments whose color code is given in panel a).

The time evolution of the fraction of atoms belonging to the different ten SOAP environments is shown in Fig. S37a together with the fraction of crystalline atoms

identified by the Q_4^{dot} order parameter for crystallinity. Snapshots at an early stage (0.08 ns), and at the end of the simulation are shown in Fig. S37b-c which reports the atoms colored according to the chemical species on the left and according to the SOAP environment on the right. The results are very similar to those of GST523 and GST9.625. First, a separation into amorphous (supercooled liquid) GeTe-like and Ge-Sb-like regions is observed and then, after the phase separation was completed, crystal nucleation and growth was observed within the GeTe-like regions. A slightly Sb-doped cubic GeTe crystal percolates through the simulation cell along the three directions (see Fig. S37b-c).

The products of the crystallization and phase separation of GST725 on the ns time scale are thus crystalline $Ge_{12}SbTe_{12}$ (slightly Sb-doped GeTe) and amorphous $Ge_{54}Sb_{46}$, instead of the thermodynamically favored Ge and GST225 crystals.

References

[1] D. Baratella, O. Abou El Kheir, M. Bernasconi, Crystallization kinetics in Ge-rich Ge_xTe alloys by large scale simulations with a machine-learned interatomic potential, Acta Materialia 284 (2025) 120608.

[2] W. K. Njoroge, H.-W. Wöltgens, M. Wuttig, Density changes upon crystallization of ge 2 sb 2.04 te 4.74 films, Journal of Vacuum Science & Technology A: Vacuum, Surfaces, and Films 20 (1) (2002) 230–233.

[3] O. Abou El Kheir, L. Bonati, M. Parrinello, M. Bernasconi, Unraveling the crystallization kinetics of the $Ge_2Sb_2Te_5$ phase change compound with a machine-learned interatomic potential, npj Comput. Mater. 10 (2024) 33.

[4] M. Rizzi, N. Ciocchini, S. Caravati, M. Bernasconi, P. Fantini, D. Ielmini, Statistics of set transition in phase change memory (PCM) arrays, in: 2014 IEEE International Electron Devices Meeting, 2014,, p. 29.6.1.

[5] B. J. Kooi, J. T. M. De Hosson, Electron diffraction and high-resolution transmission electron microscopy of the high temperature crystal structures of $Ge_xSb_2Te_{3+x}$ (x=1,2,3) phase change material, Journal of Applied Physics 92 (7) (2002) 3584–3590.

[6] O. Abou El Kheir, D. Dragoni, M. Bernasconi, Density functional simulations of decomposition pathways of Ge-rich GeSbTe alloys for phase change memories, Phys. Rev. Mater. 5 (2021) 95004.

[7] G. E. Ghezzi, J. Y. Raty, S. Maitrejean, A. Roule, E. Elkaim, F. Hippert, Effect of carbon doping on the structure of amorphous GeTe phase change material, Appl. Phys. Lett. 99 (2011) 151906.

[8] P. Zalden, C. Bichara, J. van Eijk, C. Braun, W. Bensch, M. Wuttig, Atomic structure of amorphous and crystallized ge15sb85, Journal of Applied Physics 107 (10) (2010).

[9] K. J. Singh, R. Satoh, Y. Tsuchiya, Structural changes and compound forming effects in the molten sb–te system investigated by molar volume and sound velocity measurements, Journal of the Physical Society of Japan 72 (10) (2003) 2546–2550.

[10] Y. Zheng, Y. Cheng, M. Zhu, X. Ji, Q. Wang, S. Song, Z. Song, W. Liu, S. Feng, A candidate zr-doped sb2te alloy for phase change memory application, Applied Physics Letters 108 (5) (2016).

[11] K. Laaziri, S. Roorda, J. Baribeau, Density of amorphous Si_xGe_{1-x} alloys prepared by high-energy ion implantation, J. Non-Cryst. Solids 191 (1995) 193–199.

[12] A. Crawley, D. Kiff, The density and viscosity of liquid antimony, Metallurgical Transactions 3 (1) (1972) 157–159.

[13] D. Dragoni, J. Behler, M. Bernasconi, Mechanism of amorphous phase stabilization in ultrathin films of monoatomic phase change material, Nanoscale 13 (38) (2021) 16146–16155.

[14] C. Li, C.-H. Su, S. Lehoczky, R. Scripa, B. Lin, H. Ban, Thermophysical properties of liquid te: Density, electrical conductivity, and viscosity, Journal of applied physics 97 (8) (2005).

[15] M. Schumacher, H. Weber, P. Jóvári, Y. Tsuchiya, T. G. Youngs, I. Kaban, R. Mazzarello, Structural, electronic and kinetic properties of the phase-change material $Ge_2Sb_2Te_5$ in the liquid state, Sci. Rep. 6 (2016) 1.